8-2006

On the Measurement of Yield Strength by Spherical Indentation

Erik G. Herbert
University of Tennessee - Knoxville

To the Graduate Council:

I am submitting herewith a thesis written by Erik G. Herbert entitled "On the Measurement of Yield Strength by Spherical Indentation." I have examined the final electronic copy of this thesis for form and content and recommend that it be accepted in partial fulfillment of the requirements for the degree of Master of Science, with a major in Materials Science and Engineering.

George M. Pharr, Major Professor

We have read this thesis and recommend its acceptance:

Warren C. Oliver, Carl J. McHargue

Accepted for the Council:
Carolyn R. Hodges

Vice Provost and Dean of the Graduate School

(Original signatures are on file with official student records.)

To the Graduate Council:

I am submitting herewith a thesis written by Erik G. Herbert entitled “On the Measurement of Yield Strength by Spherical Indentation.” I have examined the final electronic copy of this thesis for form and content and recommend that it be accepted in partial fulfillment of the requirements for the degree of Master of Science, with a major in Materials Science and Engineering.

George M. Pharr
Major Professor

We have read this thesis
and recommend its acceptance:

Warren C. Oliver

Carl J. McHargue

Accepted for the Council:

Anne Mayhew
Vice Chancellor and
Dean of Graduate Studies

(Original signatures are on file with official student records.)

On the Measurement of Yield Strength by Spherical Indentation

A Thesis
Presented for the
Master of Science
Degree
The University of Tennessee, Knoxville

Erik G. Herbert
August 2006

Abstract

Over the past 10 years, a number of investigators have proposed methods to measure the yield strength of metals using instrumented indentation experiments performed with a sphere [1-6]. Among the proposed methods that are easy to implement experimentally and do not require any additional novel characterization techniques or proprietary software analysis are those of Field and Swain, Yu and Blanchard, Ma et al., Cao and Lu, Kogut and Komvopoulos, and Lee, Lee, and Pharr. However, these methods have yet to be rigorously verified experimentally. The objectives of this work are twofold: first, identify the basic principles, predictions, data analysis routine, and potential experimental obstacles of each proposed method, and second, contribute to the experimental verification of four of the six methods by testing their ability to accurately predict the yield strength of the aluminum alloy 6061-T6. Tensile and indentation samples were taken from the same 3.175 mm thick sheet and the surface of the indentation sample was given the best possible mechanical polish. The indentation experiments were performed using a 90 degree diamond cone with a mechanically polished radius of 385 nm. Field and Swain's procedure overestimated the tensile flow curve by roughly 40% which precluded obtaining a meaningful estimate of the yield strength. Yu and Blanchard's model overestimated the yield strength by approximately 55%. The procedures proposed by Ma et al., and Cao and Lu were inconsistent with the experimental observations and could not be implemented. Among the most likely explanations for these surprisingly poor results are the effects of roughness and contaminants on the surface and an indentation size effect.

Table of Contents

List of Figures

1. Introduction

One of the most critical characteristics of a metal is the stress at which plastic deformation or yielding is observed to begin. From a design point of view, the stress required to produce yielding must often be completely avoided. Conversely, from a forming point of view, the stress required to produce yielding is the very basis of the process. Yielding and plasticity can also be used to decrease a material's sensitivity to surface defects that might otherwise lead to catastrophic failure. An accurate measurement of the yield strength, σ_y, is thus a prerequisite to the appropriate utilization of metals.

It is important to note that unlike the elastic modulus, *E*, yield strength is not an intrinsic material property. Yielding is produced by the motion of dislocations driven by shear stresses acting on a slip plane in a slip direction. Consequently, yielding is directly affected by the microstructure of the material and the presence of barriers to the motion of dislocations. In fact, the yield strength of a number metals can be changed by two to three orders of magnitude by controlling dislocation mobility through parameters such as the grain size and dislocation density and the addition of second phase particles and solute atoms.

Traditionally, yield strength is measured by precisely controlling the sample geometry and subjecting it to uniform stresses and strains under uniaxial tension or compression. Under these conditions, the mechanics responsible for controlling the material's response to the applied load are well understood. Measures of yielding can be assessed several ways. The true elastic limit occurs at extremely small strains (on the order of 2.0×10^{-6}) and corresponds to the motion of perhaps only a few hundred dislocations. The proportional limit occurs at larger strains and is defined as the highest stress at which the stress is directly proportional to the strain. The yield strength, by convention, is defined as the stress required to produce 0.2% plastic strain. Unfortunately, performing uniaxial tensile or compression experiments on thin films, surface treatments, or microscopic devices is at best impractical and at worst currently not possible.

Over 100 years ago, Brinell was one of the first to point out that indentation provides a very simple way of comparing the yield strength of metals [1]. Since that time, a number of investigators have employed extremely clever experimental techniques and developed rigorous mechanics models to help further our understanding of the relationship between hardness and yield strength. Unfortunately, unlike the uniform state of stress and strain produced in a tensile experiment, the stress and strain fields produced by an indentation experiment are horribly complex. As such, there is no well accepted technique that predicts the yield strength of metals from an indentation experiment.

Among investigations of the relationship between hardness and yield strength, one of the most widely cited works in the open literature is the empirical analysis of Tabor [2]. Realizing the need for a quantitative connection between the uniaxial stress-strain relationship and the hardness of metals, Tabor used a simple yet remarkably clever set of experiments to relate the two. Using blocks of annealed copper and mild steel, Tabor was able to correlate the hardness measured just inside the edge of the residual impression of a spherical indent to the yield strength of the material. He also found a reasonably strong correlation between the strain and the ratio of the diameter of the residual impression to the diameter of the indenter. By way of these correlations, Tabor developed a direct means of predicting the flow stress of metals from hardness measurements performed with a sphere. However, his analysis is only valid in the limit of fully developed plasticity and as noted, the correlation is between hardness and flow stress, not the actual yield strength. Nevertheless, his experimental observations are a cornerstone in the past 50 years of investigation.

Another important work in developing the relationship between hardness and yield stress is Johnson's expanding cavity model, which focuses on the transition regime between perfectly elastic and fully developed plasticity [3]. Specifically, the model explains how the ratio of hardness to yield stress varies with the ratio of elastic modulus to yield strength and β for an elastic-plastic contact, where β is the angle of inclination between the indenter and the surface

at the edge of the indentation (β is a measure of the intensity of strain associated with the deformation). In presenting his model, Johnson separated the contact into three discrete mechanics regimes: elastic, elastic-plastic, and fully developed plasticity. Since the model's introduction in 1970, it has become commonplace to discuss the contact mechanics in an indentation experiment from the perspective of Johnson's three regimes. They will be referred to extensively in this work in an effort to clearly communicate what type of experimental data is applicable to a given model. Figure 1 illustrates Johnson's three contact mechanics regimes [3].

Unlike pointed indenters, spheres possess the unique ability to transition through each of the three regimes. As a result, the techniques developed to measure the yield strength of metals by spherical indentation may be based on the theory of elasticity, rigid-plastic deformation (slip-line-field theory), numerical analysis, and/or empirical observation. This simple if not intuitive observation points to a fundamental aspect of measuring the yield strength of metals by spherical indentation: in order to evaluate experimental data according to a specific method, the acquired data must be representative of the regime from which the method is based: elastic, elastic-plastic, or fully developed plasticity. Because of this, methods used to predict the yield strength of metals may have limited applicability as well as unique experimental challenges associated with generating the requisite data representative of the regime from which the method is based.

While spheres do possess the unique ability to transition through all three of Johnson's regimes, it is the combination of the radius of the tip, R, and the ratio of elastic modulus to yield strength, E/σ_y, that physically determines the depth at which the transition is made from one regime to the next. Moreover, the combination of R and E/σ_y determines which of Johnson's three mechanics regimes controls how the deformation is accommodated. For example, consider a material with a large value of E/σ_y. A small radius sphere will minimize the depth of each transition and generate an unconstrained plastic contact at a more

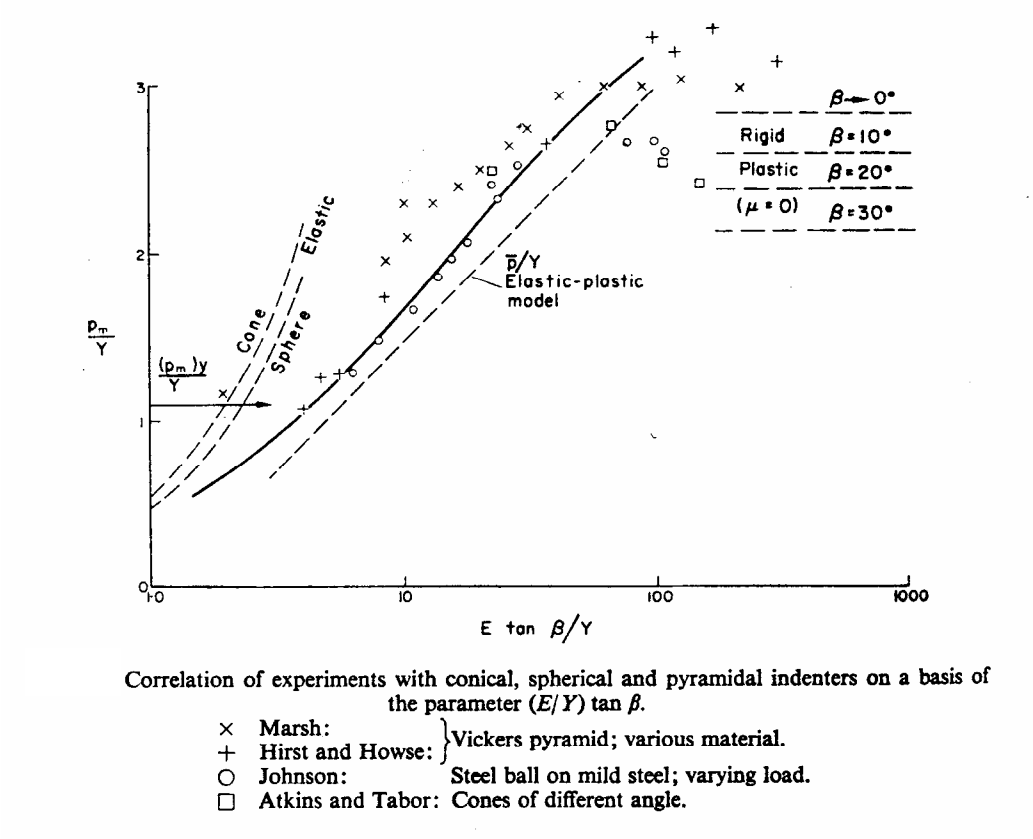

Correlation of experiments with conical, spherical and pyramidal indenters on a basis of the parameter $(E/Y)\tan\beta$.

× Marsh: } Vickers pyramid; various material.
\+ Hirst and Howse: }
○ Johnson: Steel ball on mild steel; varying load.
□ Atkins and Tabor: Cones of different angle.

Figure 1. Taken from Johnson, the ratio of hardness to yield strength as a function of $E/\sigma_y \tan\beta$ [3]. The discrete mechanics regimes are identified elastic, elastic-plastic, and rigid plastic.

shallow depth, thereby producing a contact that evolves so rapidly as a function of displacement that it is almost entirely dominated by plasticity. Conversely, for the same material, a larger sphere will increase the depth at which each transition occurs and thereby produce a contact that more gradually evolves through each of Johnson's three regimes. In considering the evolution of the contact for a material with a small value of E/σ_y, the most difficult regime to reach is that of unconstrained plasticity. The limiting factor in reaching unconstrained plasticity is the maximum achievable load of the instrument. Experimentally, when this limit is reached, the only way to move towards or further into fully developed plasticity is to achieve higher strains by using a smaller radii sphere. In either case, roughness and contaminants on the surface also play a critical role in determining how well a given method can be implemented. In order to confidently rely on the experimental load-displacement data, the surface roughness must be small in comparison to the depth of penetration, as nearly all models are based on the assumption of an intimate, single point contact between the tip and sample.

The techniques presented in this work for estimating the yield strength using nanoindentation experiments performed with spheres are based on mechanics principles taken from the theory of elasticity, rigid-plastic deformation (slip-line field theory), numerical analysis, and/or empirical observation. As a result, each method presented in this work faces unique challenges associated with generating experimental data that is representative of the mechanics model from which the method is based. Johnson's idea of breaking down the contact into three discrete mechanics regimes provides an excellent framework to compare and contrast spherical indentation techniques and their sensitivity to various experimental obstacles.

The methods selected for this study are that of Field and Swain, Yu and Blanchard, Ma et al., Cao and Lu, Kogut and Komvopoulos, and Lee, Lee, and Pharr [4-9]. While there have certainly been many more investigations performed on this topic over the past 10 years, these methods were selected for

two specific reasons: first, despite being based on markedly different mechanics principles they share exactly the same goal, prediction of the yield strength of metals by instrumented indentation performed with a sphere, and second, they each offer a means of identifying the yield strength by solely analyzing the indentation data; no other novel characterization techniques or proprietary software is required. The objectives of this work are twofold: first, identify the basic principles, predictions, data analysis routine, and potential experimental obstacles of each proposed method, and second, contribute to the experimental verification of these models by testing their ability to accurately predict the yield strength of the aluminum alloy 6061-T6.

Al 6061-T6 was chosen for this study because it is a very common engineering material with a well defined yield strength. In a manner consistent with typical surface preparation techniques, the surface of the indentation sample was given the best possible mechanical polish. The mechanical polishing may work harden the near surface region of the sample, and as a result, affect the indentation data in a manner that is completely unaccounted for in the modeling. However, as will be demonstrated, the work hardening ability of 6061-T6 is not sufficient to account for the discrepancies observed in the experimental results.

From a historical perspective, the original ideas and concepts behind the relationship between tensile and indentation data were developed based on experiments performed using spheres with radii on the order of millimeter [2 and 10]. The natural inclination of investigators using instrumented indentation, however, is to perform experiments using the smallest radii spheres possible. The motivation for using smaller spheres is simply the opportunity to probe increasingly smaller volumes of materials such as individual phases and grains or thin films on substrates. Therefore, for this investigation, the tip radius was chosen to be near the practical limit of what can be produced through mechanical polishing. The tip was made from a 90 degree diamond cone onto which a spherical tip was ground with a nominal radius of 500 nm. As will be demonstrated, the experimentally measured radius was 385 nm.

In order to test each model's ability to accurately determine the yield strength of 6061-T6, the following three experimental measurements were made: measurement of the true stress vs. true strain behavior of the alloy in uniaxial tension, measurement of the radius of the indenter tip, and measurement of the alloy's response to an indentation experiment performed with a sphere.

In applying the conclusions of past modeling and experimental investigations to small volumes of material, instrumented indentation (IIT) is what makes the experiments viable. IIT does not rely on physical measurements of the residual impression, as was necessarily done in the past. All of the critical parameters, namely the contact area and the elastic contact stiffness, are determined based on modeling the materials measured response to the applied load. Commercially available instruments are capable of routinely performing experiments on a sub-nanometer displacement scale with a load resolution of less than one micro-Newton.

2. Proposed methods

2.1 The method of J. S. Field and M. V. Swain, 1995

The primary objective of Field and Swain was to put forth an experimental method based on stepwise loading of a spherical indenter that could be used to produce a representative stress-strain curve and investigate strain hardening without having to rely on physical measurements of the residual impression. A critical component of their method is based on the assumption that if a material obeys power law hardening, it is possible to use the work hardening index, n, to account for the piling-up or the sinking-in of the contact perimeter. While their proposed method does not specifically identify the yield strength, assuming the elastic modulus is known and a portion of the stress-strain curve can accurately be determined, then the intersection of the two curves can be used to provide an estimate of the yield strength.

Based on stepwise loading, Field and Swain [11] demonstrated that the depth of the residual impression relative to the original surface after fully unloading, h_r, is given by

$$h_r = \frac{rh_s - h_t}{r - 1}, \tag{1}$$

where h_t is the depth of penetration at the peak load of each cycle, P_t, h_s is the partially recovered depth at 50% of the peak load of each cycle, P_s, and

$$r = \left(\frac{P_t}{P_s} \right)^{2/3}. \tag{2}$$

The elastic component of the displacement at each load step, h_e, is expressed as

$$h_e = h_t - h_r, \tag{3}$$

and the elastic contact stiffness at each load step, S, is determined by

$$S = \frac{3P}{2h_e}. \tag{4}$$

The depth of penetration below the contact circle in the original plane of the surface at each step, h_b, is expressed as

$$h_b = h_r + \frac{h_e}{2} \tag{5}$$

and thus, based on the geometry of a sphere, the radius of contact in the original plane of the surface, *a*', is given by

$$a' = \sqrt{2Rh_b - h_b^2}\,. \tag{6}$$

Once *a*' is determined for each cycle in the load-displacement data, the next step is to perform a linear regression of log (*P*) versus log (*a*') to examine the assumption of power law hardening. Power law hardening is assumed to be a valid assumption if the correlation is high and the slope is between 2.0 and 2.6 as suggested by Tabor [2]. The slope of the linear regression is Meyer's index *m*, which equals *n*+2 where *n* is the work hardening exponent based on the definition $\sigma = K\varepsilon^n$, where σ is the stress, ε is the strain, and *K* is the strength coefficient. Using the work hardening index obtained from the linear regression, the correction factor to account for pile-up or sink-in is determined from the proposed numerical invariant c^2, taken from Hill et al. [12],

$$c^2 = \frac{5}{2}\left(\frac{2n-1}{4n+1}\right). \tag{7}$$

The contact radius at each step, *a*, is determined by

$$a = a'c \tag{8}$$

and the depth below the circle of contact, h_c, is given by

$$h_c = c^2 h_b\,. \tag{9}$$

Finally, the representative stress, σ_r, and the representative strain, ε_r, are defined in accordance with the empirical observations of Tabor:

$$\sigma_r = \frac{P}{2.8\,\pi (ca')^2} \tag{10}$$

and

$$\varepsilon_r = 0.2\frac{ca'}{R}. \tag{11}$$

Based on stepwise load-displacement data, the technique proposed by Field and Swain predicts a representative stress-strain curve and the work hardening index of the test material. With respect to Johnson's three contact regimes, Field and Swain's technique is only applicable to data that is representative of fully developed plasticity, as the slope of the regression line of Log (*P*) versus log (*a*') can only be linear and in the range of 2.0 to 2.6 in the limit of fully developed plasticity [2]. However, it should also be noted that if the ratio of *a*/*R* is too large, friction may affect the shape of the curve in a manner not considered in their modeling. Because the slope of Log (*P*) versus log (*a*') plays a critical role in the application of their method, a simple qualitative check of the result is merited to determine whether or not the proposed analysis is valid. By profiling the residual impression it is possible to confirm whether or not the model is accurately predicting pile-up or sink-in. If the slope of Log (*P*) versus log (*a*') predicts $c > 1$, then the contact perimeter should reflect pile-up in the measured profile of the residual impression. Conversely, if the slope of Log (*P*) versus log (*a*') predicts $c \leq 1$, there should be no evidence of pile-up in the measured profile of the residual impression. If the profile is consistent with the determined value of *c*, the proposed technique may produce an accurate correction factor. On the other hand, if the measured profile is not consistent with the determined value of *c*, the analysis procedure is not valid. In instances where the proposed technique does not accurately account for pile-up or sink-in, Field and Swain suggest determining the contact area using Sneddon's stiffness equation,

$$E_r = \frac{\sqrt{\pi}}{2}\frac{S}{\sqrt{A}} = \left(\frac{1-\upsilon_i^2}{E_i} + \frac{1-\upsilon_s^2}{E_s}\right)^{-1}, \tag{12}$$

where E_r is the reduced elastic modulus, S is the elastic contact stiffness, A is the projected area of contact, υ_i and υ_s are Poisson's ratio of the indenter and the sample respectively, and E_i and E_s are Young's modulus of the indenter and the sample respectively [10]. While this is a simple and reliable means of properly

accounting for both pile-up and sink-in behavior, it does, however, require assuming values for the elastic modulus and Poisson's ratio of the sample.

By virtue of the proposed stepwise load-time history and the necessity to generate data representative of fully developed plasticity, the primary experimental obstacles to this technique are thermal drift, the potential lack of access to relatively high loads, and possibly the instrument frame stiffness. The stepwise loading procedure, with the recommended 40 to 80 cycles, requires substantially more time to run than a single load-unload experiment. The excessive time makes it more difficult to accurately account for thermal drift because the inherent assumption is that the drift rate, whether measured at the beginning or the end of the experiment, is in fact constant throughout the duration of the test. Thus, the more time the experiment takes, the less likely the assumption is valid. Since the technique proposed by Field and Swain can only be applied to data representative of unconstrained plasticity, its application may be limited to relatively small spheres, as larger spheres will require access to higher loads, which may or may not be achievable. In addition, because the smaller spheres are more difficult to accurately manufacture, it is imperative that the radius of the tip be measured experimentally. In achieving the requisite condition of unconstrained plasticity, it is possible that high modulus materials will produce contact stiffnesses that are comparable in magnitude to the instrument frame stiffness. Under these circumstances, it is extremely important to know the precise value of the instrument load frame stiffness, as it will have a dramatic affect on the final shape of the load-displacement curve.

2.2 The method of W. Yu and J. P. Blanchard, 1996

In the limit of an elastic-plastic contact, Yu and Blanchard set out to develop analytical relationships among hardness, yield stress, elastic modulus, Poisson's ratio, and indenter geometry for materials idealized as elastic perfectly-plastic. By combining the pressure distribution predicted by elastic theory and

the pressure distribution predicted by slip-line-field theory, Yu and Blanchard proposed an approximate pressure distribution that allows the yield strength to be predicted based on hardness measurements representative of an elastic-plastic contact. Their end result is a piecewise expression with natural limits that are consistent with an elastic contact as well as a rigid-plastic contact. In addition, their solution has the added benefit of being a function of a/R; thus the constraint factor (p_m/σ_y, where $p_m = P/A$ and P is the applied load) is not taken to be a constant. Integrating over their combined pressure distribution with respect to the radial position and making the appropriate substitutions, they find

$$H = \frac{-18.94(R-0.1730a)\begin{pmatrix} R^2(\upsilon^2-1)^2\sigma_y{}^2 - 0.3459aR(\upsilon^2-1)^2\sigma_y{}^2 + \\ 0.0299a^2(\upsilon^4\sigma_y{}^2 - 2\upsilon^2\sigma_y{}^2 + \sigma_y{}^2 - 5.021E^2)\end{pmatrix}\sigma_y}{a^2E^2R}, \quad (13)$$

where H is the hardness, and ν is Poisson's ratio of the sample.

Based on combining the elastic and rigid plastic pressure distribution, Yu and Blanchard developed a theoretical pressure distribution that predicts the yield strength based on hardness measurements representative of Johnson's second regime, an elastic-plastic contact. In the limit that the material does not exhibit significant work hardening, their model is also applicable to data representative of unconstrained plasticity. In this case, the predicted yield strength is more representative of the flow stress corresponding to the strain at which the hardness measurement was made. Despite the complicated appearance of Eq. 13, in the limit of unconstrained plasticity the expression effectively reduces to Tabor's empirical relation between the mean pressure and the yield stress with a constraint factor that varies about 2.8 with a/R and Poisson's ratio.

From an experimental point of view, this technique is advantageous because it is exceptionally easy to implement and it is not sensitive to the typical experimental obstacles such as thermal drift, surface roughness, and the instrument frame stiffness. Its drawback is simply that without a means of identifying precisely where in the acquired data the transitions from one regime to

the next take place, it is difficult to determine whether the data is actually being reduced according to their proposed model or, in the limit of unconstrained plasticity, the data is being reduced according to an overly complicated version of Tabor's empirical analysis. In addition, the technique relies on the assumption that the contact area is known, and thus makes no attempt to account for pile-up or sink-in, nor does it account for work hardening.

2.3 The method of D. Ma, C. W. Ong, J. Lu, and J. He, 2003

Using dimensional and finite element analysis as their basis, Ma et al. developed a general methodology to determine the yield strength and hardening behavior of metals by instrumented indentation performed with a sphere. Two types of material behavior were considered: 1) elastic followed by Hollomon power law hardening, and 2) elastic with linear hardening. The finite element analysis was carried out based on the assumptions of an elastic tip, frictionless contact, and an isotropic, rate independent solid that obeys the Von Mises yield criteria.

Their strategy for the evaluation of yield strength and hardening behavior is based on performing three experiments to maximum depths $h_m^{(i)}$, where i = 1 corresponds to a depth of 0.01R, i = 2 to 0.025R, and i = 3 to 0.05R. The loading portion of each of the three load-displacement curves is fitted according to the expression

$$P = P_m \left(\frac{h}{h_m} \right)^X , \tag{14}$$

where P is the applied load, h is the measured depth, h_m is the maximum measured depth, P_m is a fit value representing the maximum load corresponding to h_m and X is the fitting exponent. The initial objective of their procedure is to determine the fit parameters P_m and X for each of the three loading curves. Using the known or measured elastic modulus and the values P_m and X, Figures 2 and 3 are used to determine an initial estimate of the yield strength and the

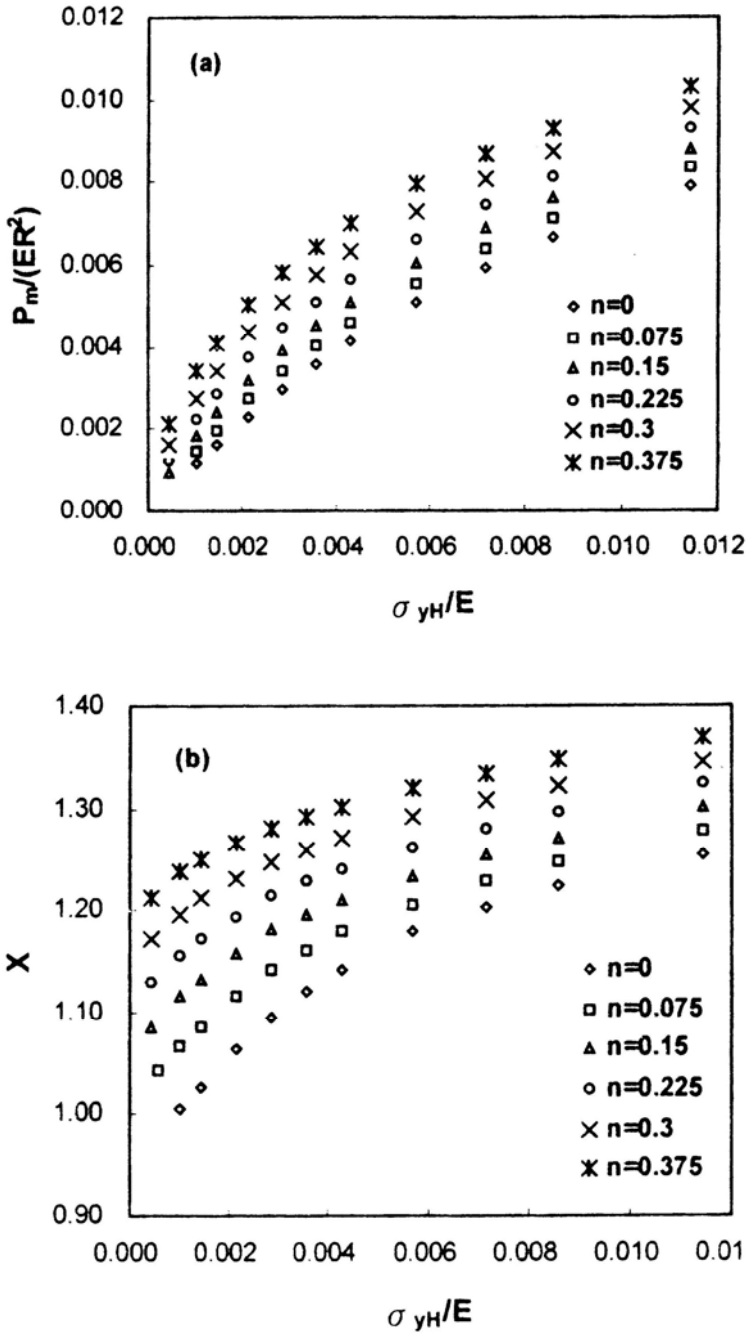

Figure 2. Taken from Ma et al., the non-dimensional scaling relationships, X and $P_m/(ER^2)$ presented as a function of σ_{yH}/E and n. The scaling relationships were derived from finite element simulations based on the assumption of linear elasticity followed by Hollomon power law work hardening.

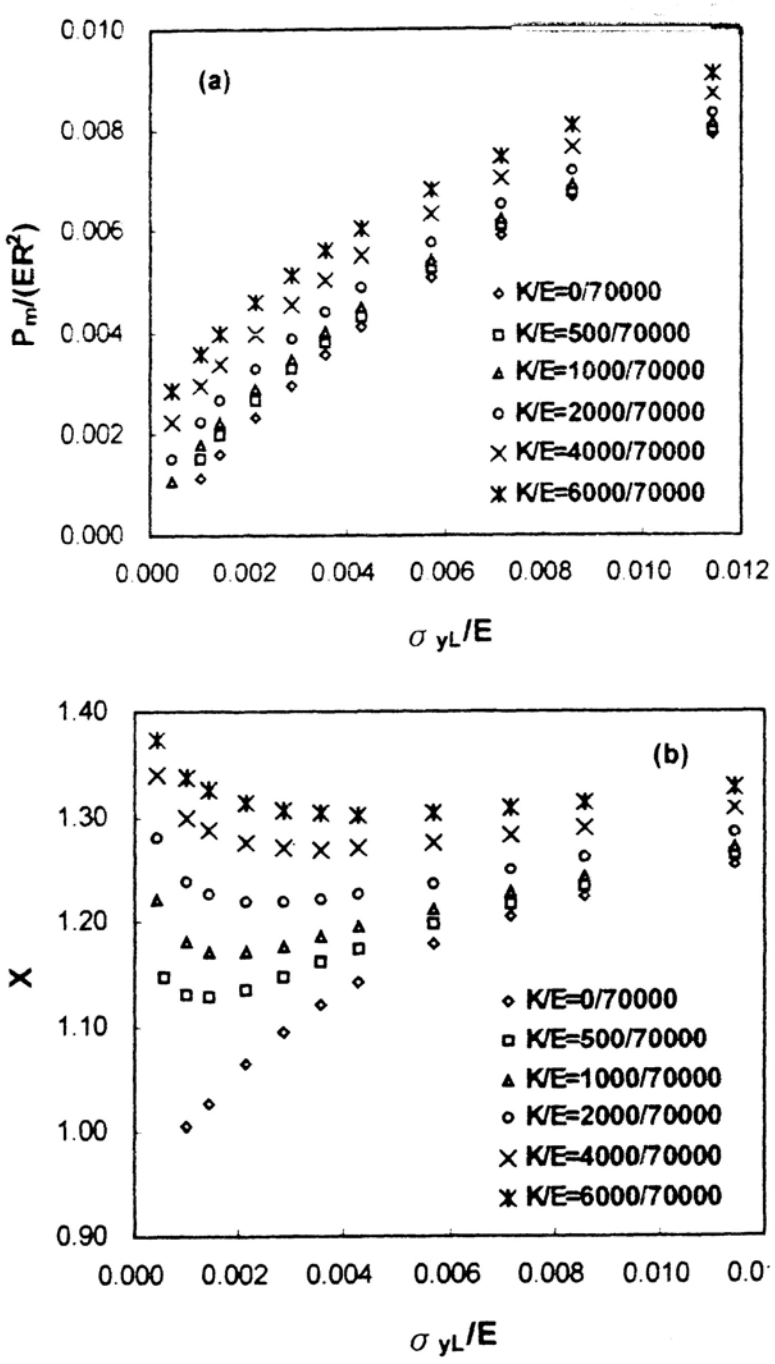

Figure 3. Taken from Ma et al., the non-dimensional scaling relationships, X and $P_m/(ER^2)$ presented as a function of σ_{yL}/E and K/E. The scaling relationships were derived from finite element simulations based on the assumption of linear elasticity followed by linear work hardening.

work hardening behavior. For a material that obeys elastic-Hollomon power law hardening, Figure 2 represents the scaling relationships expressed as

$$\frac{P_m}{ER^2} = \Phi_H\left(\frac{\sigma_{yH}}{E}, n, \frac{E_i}{E}, \frac{h_m}{R}\right) \tag{15}$$

and

$$X = \psi_H\left(\frac{\sigma_{yH}}{E}, n, \frac{E_i}{E}, \frac{h_m}{R}\right), \tag{16}$$

where σ_{yH} is the yield strength associated with Hollomon hardening. For a material that obeys elastic-linear hardening, Figure 3 represents the scaling relationships given by

$$\frac{P_m}{ER^2} = \Phi_L\left(\frac{\sigma_{yL}}{E}, \frac{K}{E}, \frac{E_i}{E}, \frac{h_m}{R}\right) \tag{17}$$

and

$$X = \psi_L\left(\frac{\sigma_{yL}}{E}, \frac{K}{E}, \frac{E_i}{E}, \frac{h_m}{R}\right). \tag{18}$$

where σ_{yL} is the yield strength associated with linear hardening and K is the work hardening modulus. Assuming the material behaves according to the elastic-Hollomon model, then the values of $\sigma_{yH}{}^{(i)}$ and $n^{(i)}$ (i = 1, 2, and 3), which are determined from Figure 2, based on the experimental data $P_m{}^{(i)}$ and $X^{(i)}$ (i = 1, 2, and 3) from the three different depths $h_m{}^{(i)}$ (i = 1, 2, and 3), should be very similar to each other while the parameters $\sigma_{yL}{}^{(i)}$ and $K^{(i)}$ (i = 1, 2, and 3) determined from the same three experiments should be different. Conversely, if the material behaves according to the elastic-linear model, then the values of $\sigma_{yL}{}^{(i)}$ and $K^{(i)}$ (i = 1, 2, and 3), which are determined from Figure 3, based on the experimental data $P_m{}^{(i)}$ and $X^{(i)}$ (i = 1, 2, and 3) from the three different depths $h_m{}^{(i)}$ (i = 1, 2, and 3), should be very similar to each other and the parameter $\sigma_{yH}{}^{(i)}$ and $n^{(i)}$ (i = 1, 2, and 3) determined from the same three

experiments should be different. At this point, their technique has produced the elastic modulus and three similar initial estimates of the yield strength as well as the hardening behavior. These data are used to achieve the final and better estimation of both the yield strength and the hardening behavior. Based on the evaluations of $\sigma_{yH}^{(i)}, n^{(i)}, \sigma_{yL}^{(i)}$, and $K^{(i)}$ from each of the three experiments, the next step is to determine the coordinates of the characteristic points. This key step in their analysis is carried out accordingly: assuming the material hardening obeys the Hollomon hardening, then the values of $\sigma_{yH}^{(1,2,3)}$ and $n^{(1,2,3)}$ are respectively the same and the elastic–Hollomon curve is plotted according to the relation

$$\sigma = \begin{cases} E\varepsilon & \varepsilon \le \varepsilon_{yH} \\ \sigma_{yH}\left(\dfrac{\varepsilon}{\varepsilon_{yH}}\right)^{n} & \varepsilon > \varepsilon_{yH} \end{cases}. \tag{19}$$

Next, the three elastic linear hardening curves are plotted with the elastic–Hollomon curve in accordance to

$$\sigma = \begin{cases} E\varepsilon & \varepsilon \le \varepsilon_{yL} \\ \sigma_{yL}^{(i)} + K^{(i)}\left(\varepsilon - \varepsilon_{yL}\right) & \varepsilon > \varepsilon_{yL} \end{cases}, \tag{20}$$

where (i = 1, 2, and 3). The characteristic points, represented by C_{ij}, are then identified by the six points of intersection between the elastic Hollomon power law curve and the three elastic linear hardening curves. The first index, i = 1, 2, and 3 corresponds to the three indentation depths $h_m^{(i)}$ and the second index, j = 1 and 2 indicates the two intersecting points corresponding to the same maximum indentation depth $h_m^{(i)}$. In the case that linear hardening is the best representation of the materials behavior, then the characteristic points would be taken to be the points of intersection between the single elastic-linear curve and the three elastic-Hollomon curves. The next step is to perform regression analysis of the six characteristic points according to Swift's power law function

$$\sigma = \alpha(\varepsilon + \varepsilon_0)^{\beta} \tag{21}$$

and evaluate the fit parameters α, β, and ε_0. Determining the final estimate of the yield strength and hardening behavior is done according to two cases:

Case 1: If $\varepsilon_0 \geq 0$, σ_y is determined by combining $\sigma = \alpha(\varepsilon + \varepsilon_0)^{\beta}$ and $\sigma = E\varepsilon$. The hardening behavior is expressed as $\sigma = \alpha(\varepsilon + \varepsilon_0)^{\beta}$ for $\varepsilon \geq \varepsilon_y = \sigma_y / E$.

Case 2: If $\varepsilon_0 < 0$, σ_y is assigned to be the ordinate of the intersecting point between the curve $\sigma = \alpha\varepsilon^{\beta}$ and $\sigma = E\varepsilon$. The stress-strain relation is divided into three regions:

1) $\sigma = E\varepsilon$ for $\varepsilon < \varepsilon_y = \sigma_y / E$

2) $\sigma = \sigma_y$ for $\sigma_y / E \leq \varepsilon \leq \sigma_y / E + \left\|\varepsilon_0\right\|$

3) $\sigma = \alpha(\varepsilon + \varepsilon_0)^{\beta}$ for $\varepsilon > \sigma_y / E + \left\|\varepsilon_0\right\|$, functions of this type are applicable to metals with an initial yield plateau.

Based on finite element analysis, the technique proposed by Ma et al. predicts the yield strength and the work hardening index of the test material. Because the load-displacement data is required to come from depths of 0.01*R*, 0.025*R*, and 0.05*R*, the technique places unrealistic expectations on experiments performed with small radii spheres, as the surface roughness must be small in comparison to the total depth in order to meet the requirement of a single point contact. In addition, the data acquired at small displacements are very sensitive to the effects of contaminants on the surface such as oxides. Without accounting for surface roughness and contaminants, it is not possible for the model to accurately predict the material behavior at displacements where the roughness and contaminants make a significant contribution to the measured load-displacement data. The end result is that the technique is not well suited towards investigating small volumes of material, such as thin films, through the use of small radii spheres. In the limit that the prescribed depth is deep enough such that roughness and contaminants on the surface do not contribute in any significant way to the acquired load-displacement data, the proposed technique

is not sensitive to the typical experimental obstacles such as thermal drift and the instrument frame stiffness.

2.4 The method of Y. P. Cao, and J. Lu, 2004

Based on a priori knowledge of the elastic modulus and using a spherical indenter to perform experiments to depths of approximately 0.01*R* and 0.06*R*, the procedure proposed by Cao and Lu attempts to uniquely determine the yield strength and the work hardening index of a material by extending the representative strain as defined by Dao et al. [13] for sharp indentation to spherical indentation. Using finite element analysis, development of their model is based on the mechanical behavior of a bulk, homogeneous, isotropic material that behaves according to linear elasticity followed by Hollomon power law work hardening.

The constitutive relations used to describe the material behavior are $\sigma = E\varepsilon$ and $\sigma = K\varepsilon^n$. When $\sigma > \sigma_y$, the flow stress can also be expressed as

$$\sigma = \sigma_y \left(1 + \frac{E}{\sigma_y} \varepsilon_f \right)^n , \tag{22}$$

where ε_f is the total effective strain accumulated beyond the yield strain.

Their measurement procedure consists of performing experiments to two different depths. Using their nomenclature, the recommended combination of depths is $h_{g,1} = 0.01R$ and $h_{g,2} = 0.06R$. The lower displacement limit is bound by the necessity to avoid deformation that is largely elastic. The upper limit is determined by the necessity to minimize the effects of friction, which become more prevalent as the depth of penetration increases.

The loads corresponding to $h_{g,1}$ and $h_{g,2}$ are recorded as $P_{g,1}$ and $P_{g,2}$. Based on their numerical analysis, the flow stresses corresponding to $P_{g,1}$ and

$P_{g,2}$ are solved for according to the relation

$$P_g = \sigma_r h_g^2 \left[C_1 \ln^3\left(\frac{E_r}{\sigma_r}\right) + C_2 \ln^2\left(\frac{E_r}{\sigma_r}\right) + C_3 \ln\left(\frac{E_r}{\sigma_r}\right) + C_4 \right], \quad (23)$$

where σ_r is the flow stress and the coefficients C_1, C_2, C_3, and C_4 are a function of h_g/R and their respective values are provided in tabular form. The next step in their analysis is to calculate the effective strain, given by

$$\varepsilon_f = 0.00939 + 0.435\frac{h_g}{R} - 1.106\left(\frac{h_g}{R}\right)^2. \quad (24)$$

Through Eqs. 23 and 24, the two experimental measurements effectively produce two points on the plastic flow curve. Using Eq. 22 in the form of two equations and two unknowns, the yield strength may be determined by solving the two equations simultaneously.

Based on finite element analysis, the technique proposed by Cao and Lu predicts the yield strength and the work hardening index of the test material. Because the load-displacement data are required to come from depths of 0.01R and 0.06R, the technique suffers from precisely the same problems associated with the technique proposed by Ma et al; it places unrealistic expectations on experiments performed with small radii spheres, as the roughness and contaminants on the surface must be a small fraction of the total displacement. As is the case with Ma et al., the technique proposed by Cao and Lu is not well suited to the evaluation of small volumes of material such as thin films. However, when the depth is deep enough such that roughness and contaminants on the surface do not contribute in any significant way to the acquired load-displacement data, the proposed technique is not uncommonly sensitive to the typical experimental obstacles of thermal drift and the instrument frame stiffness.

2.5 The method of L. Kogut, and K. Komvopoulos, 2004

Citing Hill et al. [12], Biwa and Storakers [14], Johnson [3], and Mesarovic and Fleck [15], Kogut and Komvopoulos were well aware that the constraint factor does not reach the often quoted value of 3 for materials with relatively large yield strains or small values of E/σ_y (approximately E/σ_y less than 300). By using finite element analyses to numerically model the deformation behavior of these types of materials by a rigid sphere, Kogut and Komvopoulos developed several non-dimensional expressions that provide experimentalists with a means to estimate the boundary between elastic-plastic and fully developed plasticity and subsequently the yield strength of the test material.

Their work is focused on deformation in the elastic-plastic transition regime. The reasons for this are two fold: first, for materials with sufficiently high values of E/σ_y (E/σ_y > 450), the elastic strains can be ignored and the material can be idealized as rigid-perfectly plastic, for which the similarity solution is a good approximation. Second, citing Park and Pharr [16], strain hardening exhibits a marginal response in this regime which therefore simplifies the problem by allowing the materials to be modeled as elastic-perfectly plastic.

Using finite element analysis to study the relationship between hardness and yield strength, Kogut and Komvopoulos developed the following non-dimensional expressions:

$$\frac{H}{\sigma_y} = 0.201 \ln\left(\frac{E}{\sigma_y}\right) + 1.685 , \tag{25}$$

$$\frac{\delta}{r'} = \frac{1}{1 + 0.037\dfrac{E}{\sigma_y}} , \tag{26}$$

and

$$\frac{P}{a'\sigma_y} = \frac{0.839 + \ln\left[\left(\frac{E}{\sigma_y}\right)^{0.656}\left(\frac{\delta}{r'}\right)^{0.651}\right]}{2.193 - \ln\left[\left(\frac{E}{\sigma_y}\right)^{0.394}\left(\frac{\delta}{r'}\right)^{0.419}\right]}, \tag{27}$$

where *r'* is the truncated contact radius, *a'* is the truncated contact area, and δ is the displacement. Using the known modulus and an initial estimate of the yield strength, Eqs. 26 and 27 are evaluated to determine the initial estimates of $\frac{\delta}{r'}$ and $\frac{p_m}{a'\sigma_y}$. Based on the measured radius and the following relation,

$$\frac{\delta}{r'} = \frac{\sqrt{\delta}}{\sqrt{2R-\delta}}, \tag{28}$$

the displacement is determined. Using the calculated displacement and the measured radius, the load, *P*, is determined from the following expression,

$$\frac{P}{a'Y} = \frac{P}{\pi\delta(2R-\delta)Y}. \tag{29}$$

Next, an experiment is performed to the calculated load and the corresponding depth is recorded. Based on the recorded depth, the known radius, and the following relation,

$$\frac{\delta}{r'} = \frac{\sqrt{\delta}}{\sqrt{2R-\delta}} = \frac{1}{1+0.037\frac{E}{\sigma_y}}, \tag{30}$$

a new estimate of the yield strength is determined. This procedure is iterated until convergence to a specific tolerance is reached.

Based on finite element analysis, the technique proposed by Kogut and Komvopoulos predicts the load required to initiate fully developed plasticity and the yield strength of the test material. Because the technique requires obtaining data from precisely the transition point from elastic-plastic to unconstrained plasticity, its sensitivity to roughness and contaminants on the surface will vary with the ratio of E/σ_y and the radius of the sphere. The sensitivity to roughness

and contaminants will be highest for the combination of a large value of E/σ_y and a small radius sphere, as this combination forces the transition to occur at shallow depths, where the surface roughness is more likely to be a significant fraction of the depth of penetration. On the other hand, it will be lowest for the combination of a small value of E/σ_y and a large radius sphere, as this combination forces the transition to occur at larger displacements, where the surface roughness will most likely be insignificant in comparison to the depth of penetration. One drawback of the proposed method is that the experiments cannot be automated. They are necessarily iterative in order to precisely locate the transition between elastic-plastic and unconstrained plasticity.

2.6 The method of H. Lee, J. H. Lee, and G. M. Pharr, 2005

Based on finite element analysis using incremental plasticity theory, Lee et al. developed an iterative analysis procedure that predicts the elastic modulus, the yield strength, and the work hardening exponent of the test material. The finite element analysis was carried out based on the assumptions of an elastic tip, and an isotropic, rate independent solid that obeys Von Mises yield criteria, and friction was permitted. The material was modeled according to linear elasticity followed by Hollomon power law work hardening. Regression of the finite element solutions for various material properties generated the following non-dimensional parameters, expressed using Einstein summation notation:

$$\begin{aligned} &c^2 = f_0^c(\varepsilon_0, n) + f_1^c(\varepsilon_0, n)\ln(h_t/D), \\ &f_1^c(\varepsilon_0, n) = a_{ij}(\varepsilon_0) n^{-j}, \quad i = 0, 1, \quad j = 0, 1, 2, 3, 4, \\ &a_{ij}(\varepsilon_0) = \alpha_{ijk}\varepsilon_0^k, \quad k = 0, 1, 2, 3. \end{aligned} \tag{31}$$

$$\begin{aligned} &\varepsilon_p = f_i^c(\varepsilon_0, n)(h_t/D)^i, \\ &f_i^\varepsilon(\varepsilon_0, n) = b_{ij}(\varepsilon_0) n^{-j}, \quad i = 0, 1, 2, 3, \quad j = 0, 1, 2, 3, 4, \\ &b_{ij}(\varepsilon_0) = \beta_{ijk}\varepsilon_0^k, \quad k = 0, 1, 2, 3. \end{aligned} \tag{32}$$

$$\psi = \frac{P}{D^2\sigma} = f_i^{\psi}(\varepsilon_0, n)(h_t/D)^i,$$
$$f_i^{\psi}(\varepsilon_0, n) = c_{ij}(\varepsilon_0) n^{-j}, \quad i = 0, 1, 2, 3, \quad j = 0, 1, 2, 3, 4, \tag{33}$$
$$c_{ij}(\varepsilon_0) = \gamma_{ijk}\varepsilon_0^k, \quad k = 0, 1, 2, 3.$$

where ε_0 is the yield strain, n is the work hardening exponent (based on the definition $\sigma = K\varepsilon^{\frac{1}{n}}$), h_t is the total depth of penetration, D is the diameter of the indenter, and a, b, and c are coefficients of a polynomial function. The coefficients are provided in tabular form.

Experimental load-displacement data taken to 6% of the diameter of the tip is reduced by initially assuming values for ε_0 and n and then evaluating c^2, ε_p, and ψ using Eqs. 31-33. From equation 31, d^i is given by

$$d^i = 2\sqrt{(c^2)^i h_t D - \left[(c^2)^i h_t\right]^2}. \tag{34}$$

From equations 32 and 33, σ^i is determined according to

$$\sigma^i = \frac{P}{D^2\psi^i}. \tag{35}$$

K^{i+1} and n^{i+1} are evaluated using

$$\sigma^i = K^{i+1}\varepsilon_t^{1/n^{i+1}}, \tag{36}$$

and E^{i+1} is given by

$$E = \frac{1-\upsilon^2}{d/kS - (1-\upsilon_1^2)/E_1},$$
$$k(\varepsilon_0, n) = g_j(\varepsilon_0) n^{-j}, \quad j = 0, 1, \tag{37}$$
$$g_j = \lambda_{jk}\varepsilon_0^k, \quad k = 0, 1, 2.$$

The yield strength, ${\sigma_0}^{i+1}$, and ${\varepsilon_0}^{i+1}$ are determined according to

$${\sigma_0}^{i+1} = E^{i+1}\left(\frac{K^{i+1}}{E^{i+1}}\right)^{n^{i+1}/(n^{i+1}-1)} \tag{38}$$

and ${\varepsilon_0}^{i+1} = \frac{{\sigma_0}^{i+1}}{E^{i+1}}$. (39)

The percent relative error is determined for each iteration and the procedure is repeated until the specified tolerance is reached.

Based on finite element analysis, the technique proposed by Lee, Lee, and Pharr predicts the elastic modulus, the yield strength, and the work hardening index of the test material. Because the load-displacement data is required to come from a depth of $0.06R$, the technique suffers from precisely the same problems associated with Ma et al. and Cao and Lu; it places unrealistic expectations on experiments performed with small radii spheres, as the roughness and contaminants on the surface must be a small fraction of the total displacement. As is the case with Ma et al. and Cao and Lu, the technique proposed by Lee et al. is not well suited to the evaluation of small volumes of material such as thin films. However, when the depth is deep enough such that roughness and contaminants on the surface do not contribute in any significant way to the acquired load-displacement data, the proposed technique is not sensitive to the typical experimental obstacles. However, the proposed data analysis is exceptionally tedious. In their expanded form, equations 31-33 have 40 terms each and all three equations are part of the iterative analysis. The only reasonable way to reduce experimental data according to this procedure is to build the solution into a software analysis routine.

3. Experimental measurements and procedures

3.1 Uniaxial tensile measurements

Six dog bone specimens were taken from a single 3.175 mm thick sheet by wire electrical discharge machining (EDM). The tensile experiments were conducted at room temperature using an MTS 10/GL load frame with a 44,484 N load cell and an MTS extensometer (model 63212) with a 2.54 cm gauge length. The experiments were performed with a constant engineering strain rate of approximately 10^{-2} s^{-1}.

Figure 4 illustrates the true stress vs. true strain data from one of the six experiments. For the sake of clarity, the plotted data represent only a small fraction of the total acquired data in each experiment. The average elastic modulus was determined to be 72.59 GPa ± 2.54 % and the average 0.2% offset yield strength was determined to be 273 MPa ± 0.70 %. Both are within reasonable agreement with the literature values of 69 GPa and 275 MPa respectively. In addition, Figure 4 reveals the aluminum's ability to satisfy the Hollomon power law work hardening relationship, expressed as $\sigma = K\varepsilon^n$, where σ is the stress, ε is the strain, K is the strength coefficient, and n is the work hardening index. Ignoring the elastic portion of the curve, the values of K and n were determined by fitting the plastic portion of all six true stress vs. true strain curves according to the Hollomon expression. The average values of K and n were 432.0 MPa ± 0.2 % and 0.093 ± 0.8 %, respectively. As shown in Figure 4, the power law fit clearly does a good job of matching the experimental flow curve. This observation is important because each of the models in this review are based on the assumption that the work hardening can be accurately described by the Hollomon relation. In addition, it is interesting to note that continuity at the point of yielding requires

$$K = \sigma_y \left(E / \sigma_y \right)^n \tag{40}$$

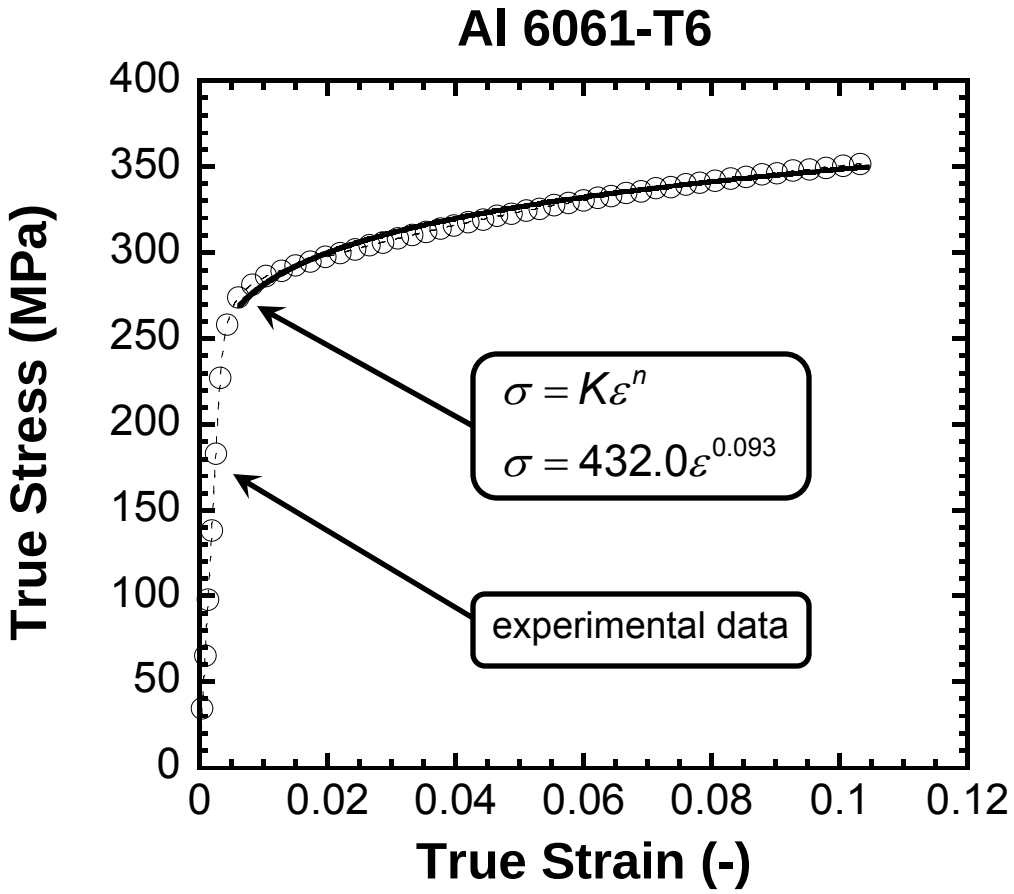

Figure 4. The true stress vs. true strain behavior of Al 6061-T6 as measured in uniaxial tension. As shown by the good agreement between the experimental data and the curve fit, the plastic portion of the data can be accurately described by the Hollomon power law work hardening relationship.

and therefore the yield strength, σ_y , determined from *K*, *n*, and the measured elastic modulus, *E*, is 255 MPa, an underestimation of 6.6%. This observation is worth pointing out because it indicates that even if the indentation data can be reduced to accurately reproduce the flow curve to very small strains, fitting the data according to an assumed power law of the form $\sigma = K\varepsilon^n$ will still lead to an underestimation of the yield strength on the order of 7%.

3.2 Determination of the indenter tip radius

A tacit assumption of the reviewed models is that the radius of the indenter tip is known and that the radius perfectly describes the geometry of the tip. Despite efforts to manufacture spherical tips as accurately as possible and given the demanding nature of the models, it is necessary to experimentally measure the radius. For this investigation, we chose to acquire data on a standard reference material that was representative of an elastic contact, then solve for the radius of the tip by reducing the data according to Hertz's elastic load-displacement relationship,

$$P = \frac{8\sqrt{2}}{3} E_r \sqrt{R} h_c^{3/2} \tag{41}$$

where *P* is the applied load, E_r is the reduced elastic modulus, *R* is the radius of the indenter tip, and h_c is the contact depth [10].

Fused silica was chosen to be the standard reference material used to determine the radius of the tip. It complies with the assumptions of Hertz's elastic load-displacement relationship, has a relatively smooth surface, and known elastic constants. Furthermore, it has a reasonably high yield strength which helps maintain an elastic contact to relatively large depths. However, that being said, it should also be noted that because of assumptions in Hertz's model, the geometry of the contact must also be accurately approximated by a parabola. This can only be done in the limit that $2h_cR >>> h_c^2$. The point is that even if the silica had an infinite yield strength, thereby maintaining an elastic contact

regardless of the depth of penetration, the resulting load-displacement data at larger depths would not be suitable for reduction according to Hertz's elastic load-displacement relationship.

Among the challenges in acquiring accurate load-displacement data is determining which portion of the data are actually representative of an elastic contact, as it depends on surface roughness and determination of the initial point of contact as well as thermal drift and measurement time constants. Figure 5 shows the experimental displacement-time history we used to help address this issue. The data were generated using a multiple load-unload experiment whereby the loading and unloading of each cycle were performed as quickly as possible, thus minimizing the impact of thermal drift. Before the load and displacement data were recorded in each cycle, the load was held constant for 8 times the measurement time constant or 1.6 s, thereby eliminating problems associated with measurement time constants. The key aspect of this experiment is that the unloading in each cycle was carried out to precisely 20 μN. For each cycle in which the deformation is dominated by elasticity, unloading to precisely 20 μN must necessarily generate displacement data that terminate at nominally the same displacement. For each of these elastic cycles, the load, contact depth, and reduced elastic modulus are known; therefore Hertz's elastic load-displacement relationship (Eq. (41)) can be used to determine the radius of the tip. The utility of this particular experiment is that it is not based on the complete reversibility of continuously recorded load-displacement data. It is based on using a single point elastic contact where the load and displacement are known. Assuming the displacement at that point is large relative to the surface roughness, this experiment is less sensitive to the effects of surface roughness and determination of the point of contact. As illustrated by Figure 5, the unloaded displacement from at least the first two cycles terminated at nominally the same value, thus suggesting that data from the first two cycles is representative of a contact dominated by elasticity. Figure 6 compares the experimentally controlled load and Hertz's elastic load-displacement relationship

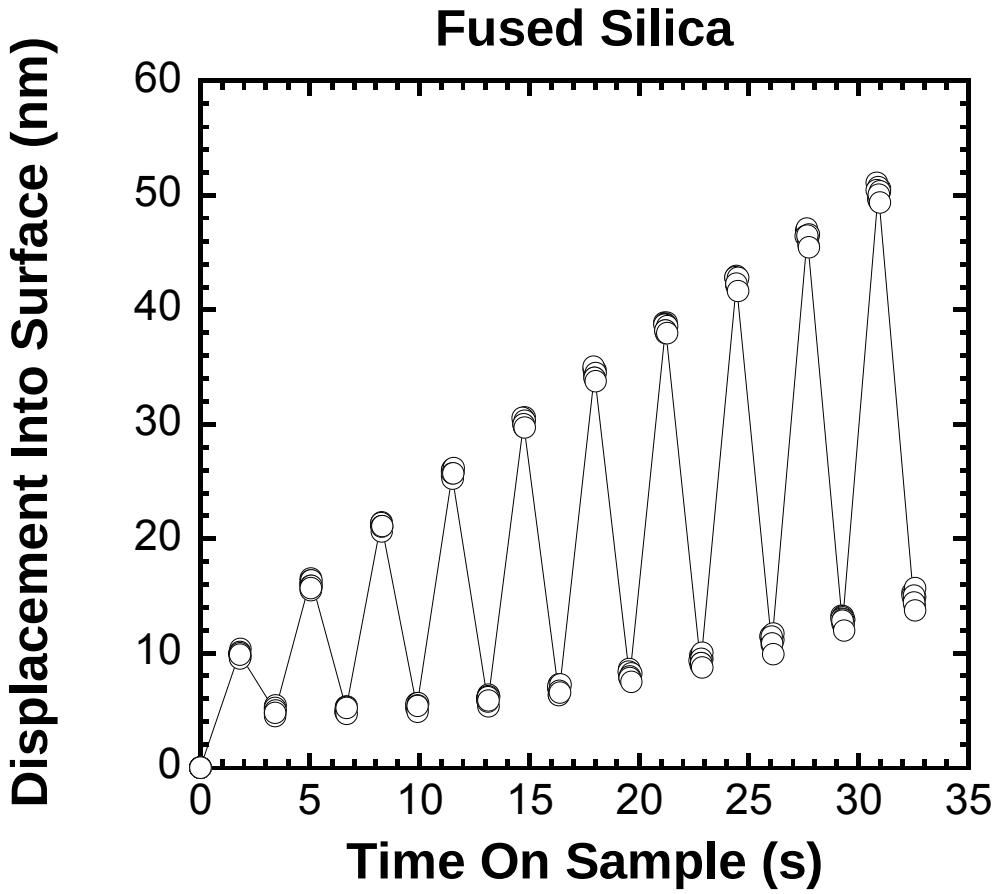

Figure 5. Displacement-time history used in determining the radius of the indenter. Given that the unloaded portion of each cycle was taken to precisely 20 μN, the displacement-time response shows that data from the first two cycles terminated at nominally the same displacement and therefore the data is representative of a contact dominated by elasticity.

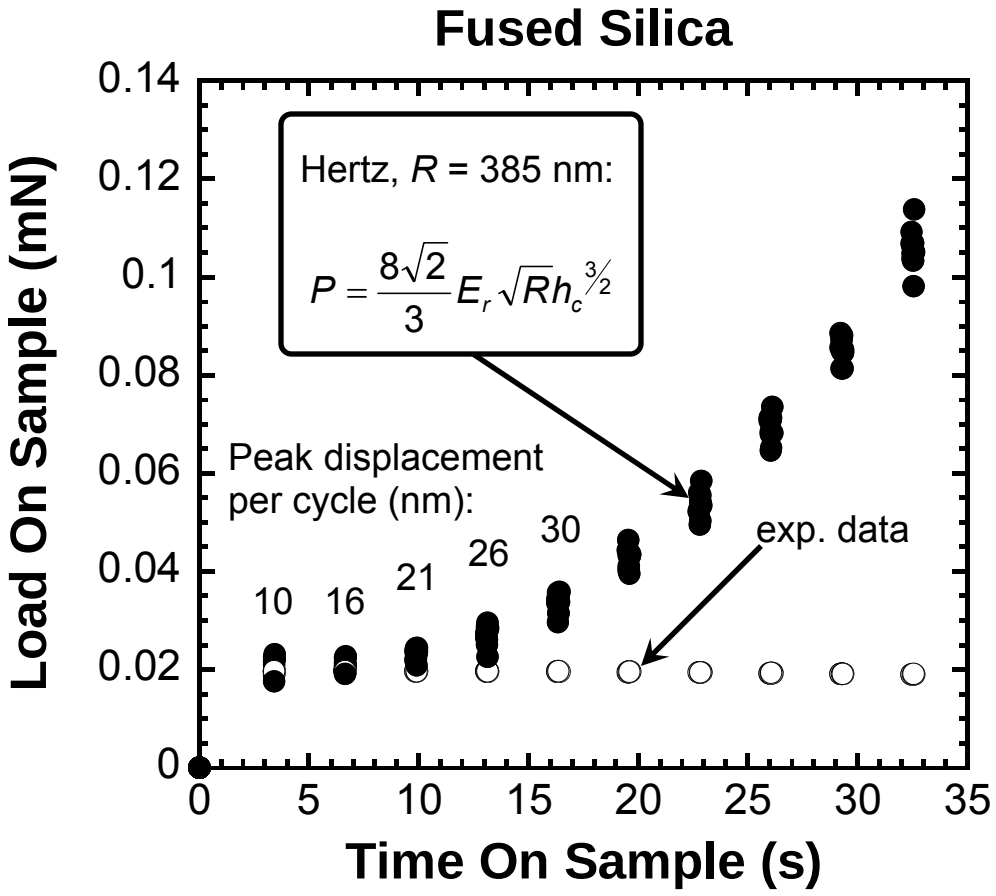

Figure 6. Load vs. time for the unloaded portion of the fused silica data used to determine the radius of the tip. In considering data from the first two load-unload cycles, a radius of 385 nm provided the best match between Hertz's elastic load-displacement relationship and the experimentally acquired data.

for all ten cycles. For the low load elastic contacts, a radius of 385 nm provides good agreement between the experimental data and Hertz's relation.

Based on this experimentally determined radius, an estimate of the yield strength of fused silica (taken from finite element simulations), and the known reduced elastic modulus, it is possible to estimate the displacement at which yielding first occurs. Assuming von Mises yield criteria and a Poisson's ratio of 0.3, it has been shown that at the point of yielding, the mean pressure is $p_m = 1.07\sigma_y$ [10]. In addition, under the same assumptions it has also been shown that the maximum shear stress occurs on the axis of symmetry beneath the surface at a depth of approximately 0.48*a*, where *a* is the contact radius [10]. Taking R = 385 nm, σ_y = 5.17 GPa, and E_r = 69.88 GPa, the estimated displacement at yielding is 13.4 nm. The peak displacements of the first five cycles are identified in Figure 6. As the deviation between the experimental data and Hertz's expression indicates, yielding appears to have occurred somewhere between 16 and 26 nm of displacement. Given that yielding does not initiate at the surface but actually initiates beneath the surface, the slightly higher experimental displacements appear to be in reasonable agreement with what would be expected theoretically. This therefore supports the conclusion that data from the first two cycles is dominated by elasticity and thus it is aptly suited for analysis according to Hertz's elastic load-displacement relationship.

3.3 Indentation data

Using wire electrical discharge machining (EDM), an indentation sample of Al 6061-T6 was taken from the same sheet as the tensile samples. All of the indentation experiments were performed using an MTS Nano Indenter® XP. The data were acquired using two different load-time histories. In the first experiment, the load was controlled such that the loading rate divided by the magnitude of the load, $\dot{P}$/P, was held constant at 0.05 s^{-1}. In addition, the continuous stiffness

measurement technique was used to directly measure the elastic contact stiffness as a continuous function of the indenter's displacement into the surface of the sample. In the second experiment, the load-time history followed the stepwise procedure outlined by Field and Swain [4]. In this experiment, 80 load and unload cycles were completed along a linear load ramp to a maximum load of 2 mN. The load was controlled such that the loading and unloading portion of each cycle both took 5 s to complete. In addition, there was a 2 s hold prior to the acquisition of load and displacement data. The unloading portion of each cycle terminated at 50% of the peak load of each cycle. For both load-time histories, measured thermal drift rates were used to correct the displacement data.

4. Implementation of the methods: results and discussion

4.1 The method of J. S. Field and M. V. Swain, 1995

The primary objective of the model developed by Field and Swain was to put forth an experimental method based on stepwise loading that could be used to produce a representative stress-strain curve and investigate strain hardening without having to rely on physical measurements of the residual impression. A critical component of their method is based on the assumption that if a material obeys power law hardening, it is possible to use the work hardening index, *n*, to account for the 'piling-up' or the 'sinking-in' of the contact perimeter and therefore accurately determine the actual contact radius. While their proposed method does not specifically identify the yield strength, knowing the elastic modulus allows one to estimate the yield strength from the intersection of the elastic and power law stress-strain relations.

Figure 7 illustrates the averaged stepwise load-displacement data acquired according to the procedure outlined by Field and Swain, and for comparative purposes, the averaged data obtained separately using $\dot{P}/P = 0.05$ s^{-1}. As illustrated by the plot, the two loading techniques produce nominally the same loading curve. However, as shown by the individual curves in Figure 8, the load-displacement data below 20 nm is compromised. Once the indenter makes contact with the surface of the sample, the applied load is supported by multiple asperities, both on the surface of the tip and the sample. As the load is increased, the asperities plastically deform and the contact geometry gradually evolves to a single point contact. During this transition from a multiple asperity contact to a single point contact, the load-displacement data is generally very scattered, as the load required to plastically deform the asperities depends on the volume of asperities supporting the tip, which varies from one experiment to the next. Once the single point contact is achieved, the load-displacement data becomes reproducible, as the data are now representative of the bulk material.

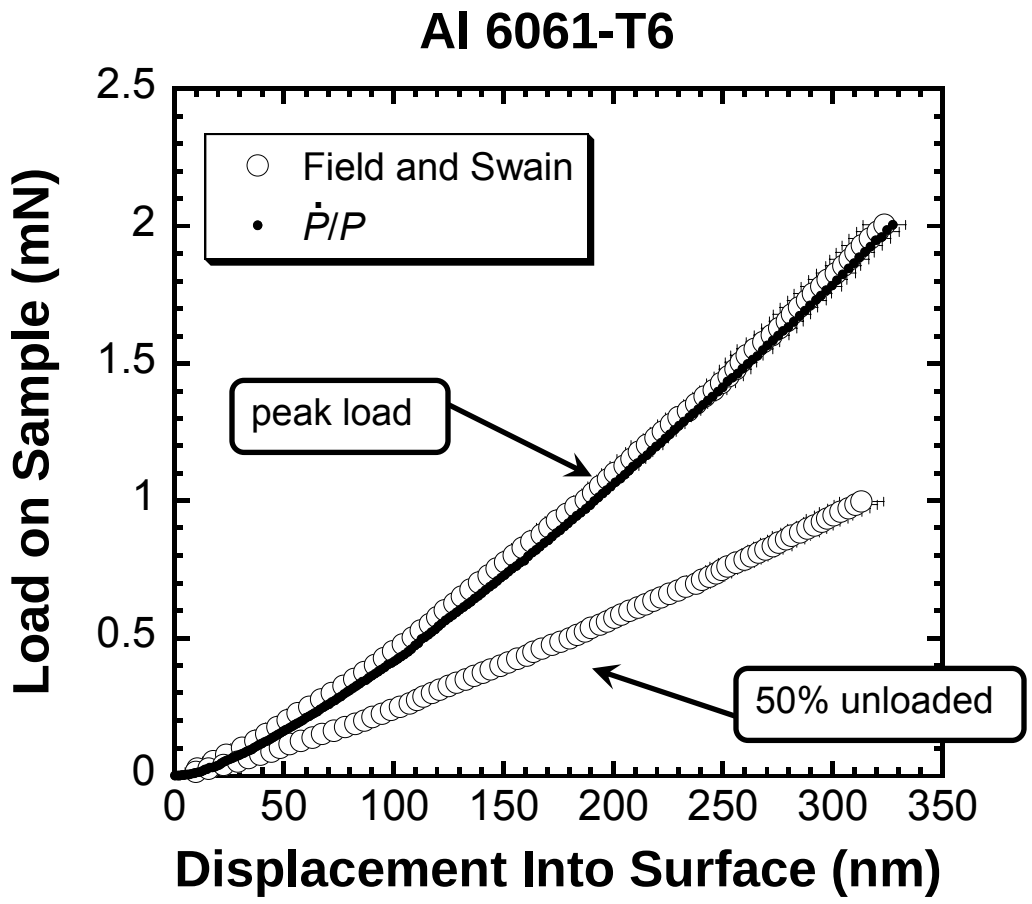

Figure 7. Averaged load vs. displacement for Al 6061-T6. The error bars span one standard deviation about the mean. Both loading techniques produce nominally the same loading curve.

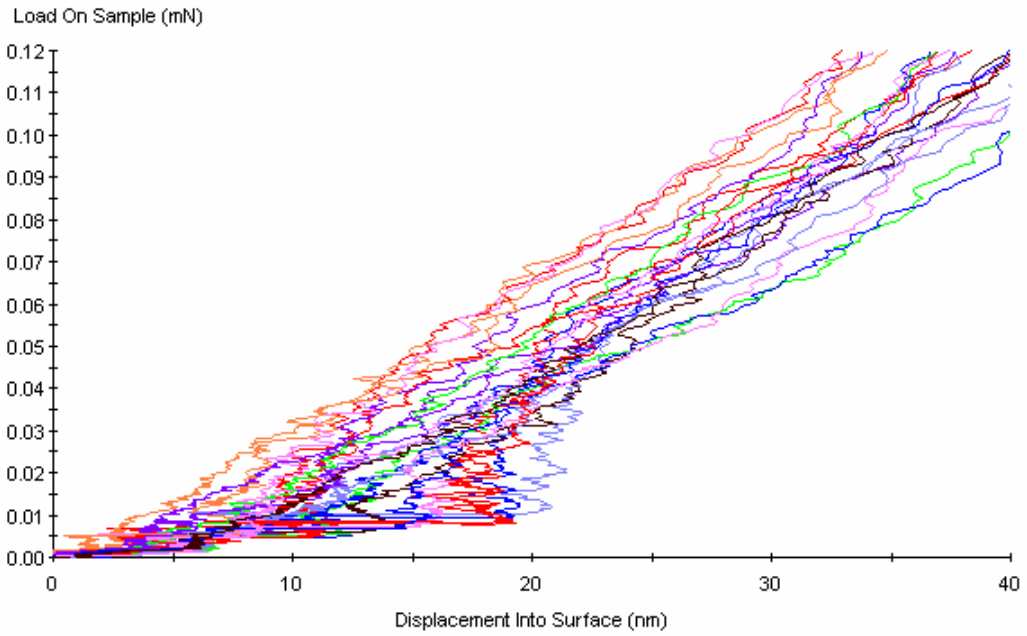

Figure 8. Load-displacement data illustrating 25 of 30 individual experiments performed on Al 6061-T6 using a 385 nm radius sphere. The additional scatter below 20 nm is due to roughness and contaminants on the surface of the tip and the sample.

As evidenced by the data in Figure 8, the depth at which the single point contact is generated is approximately 15 nm. AFM profiles of the surface, shown in Figure 9, confirm that the surface roughness is in fact approximately 15 nm, peak to peak.

Using the stepwise load-displacement data and reducing it according to Field and Swain's suggested procedure, Figure 10 illustrates the linear regression of Log *P* versus Log *a*', where *P* is the applied load and *a*' is the contact radius in the original plane of the surface. According to Field and Swain, power law hardening is assumed to be a valid assumption if the plot is linear and the slope is between 2.0 and 2.6 as suggested by Tabor [2]. The slope of the linear regression is Meyer's index *m*, which equals *n*+2 where *n* is the work hardening exponent based on the definition $\sigma = K\varepsilon^n$. Assuming the appropriate value of the work hardening index *n* is obtained from the linear regression, then the correction factor to account for pile-up or sink-in is determined from the proposed numerical invariant c^2 from Hill et al. [12],

$$c^2 = \frac{5}{2}\left(\frac{2n-1}{4n+1}\right). \tag{42}$$

As indicated by the linear regression in Figure 10, the correlation is excellent and the slope falls within the specified range; thus power law hardening is assumed to be a valid assumption. However, the work hardening exponent obtained from the slope is 0.549, which is not in good agreement with that obtained from the tensile experiments, of $n = 0.093 \pm 0.8$ %. Furthermore, the value of *c* obtained from Eq. (42) is 0.893, which predicts significant sink-in. In reality we know from AFM images of the residual impression that the contact actually exhibits significant pile-up, not sink-in as predicted by the model. This means that the procedure will grossly underestimate the actual contact area and hence overestimate the yield strength. Field and Swain did point out that some materials would not be suitable for analysis according to their procedure. In those instances, they recommended assuming a value for the elastic modulus and using Sneddon's stiffness equation (Eq. (12)) to determine the contact area.

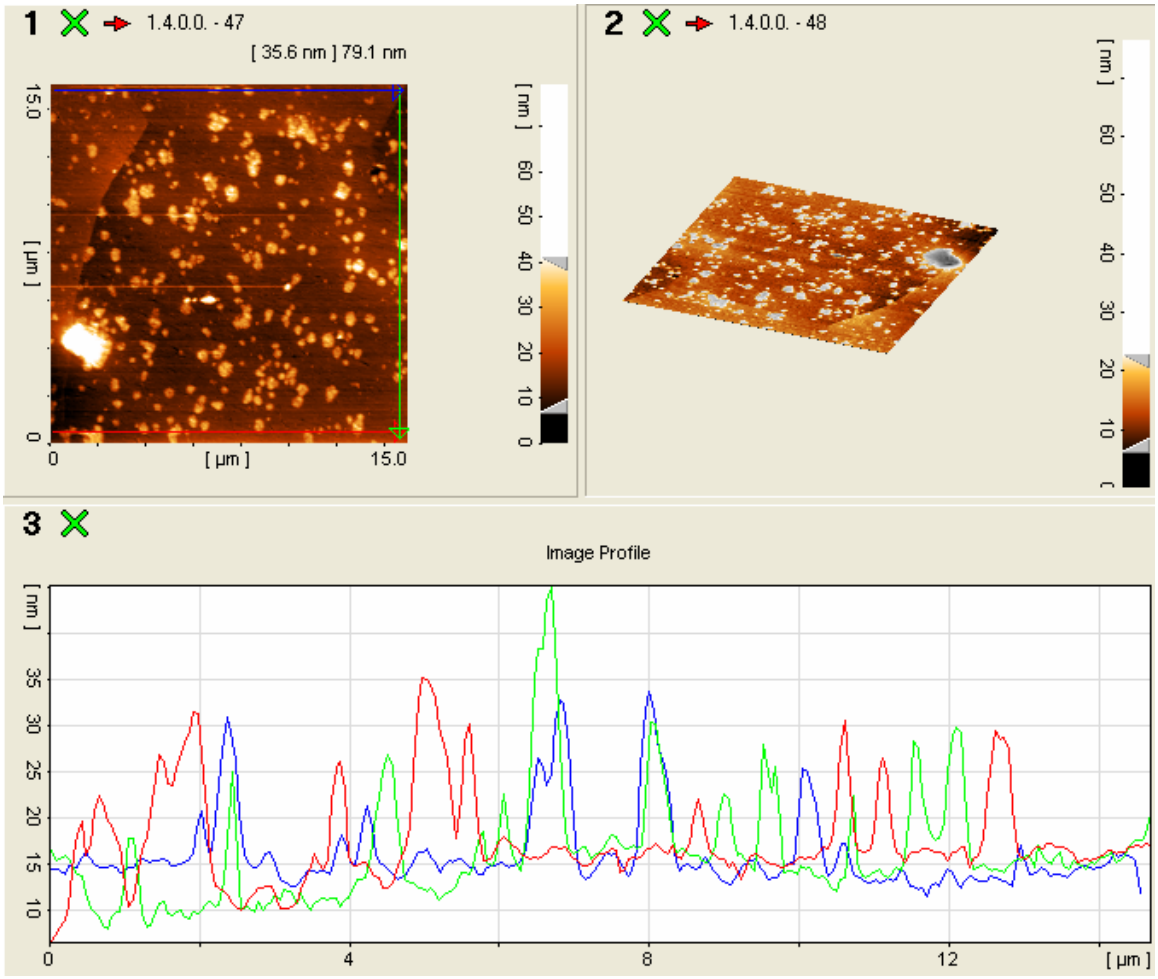

Figure 9. A 15 by 15 µm AFM image of the mechanically polished surface of Al 6061-T6. The surface roughness, as determined from the red, green, and blue profiles shown in the 2-dimensional image, is approximately 15 nm, peak to peak.

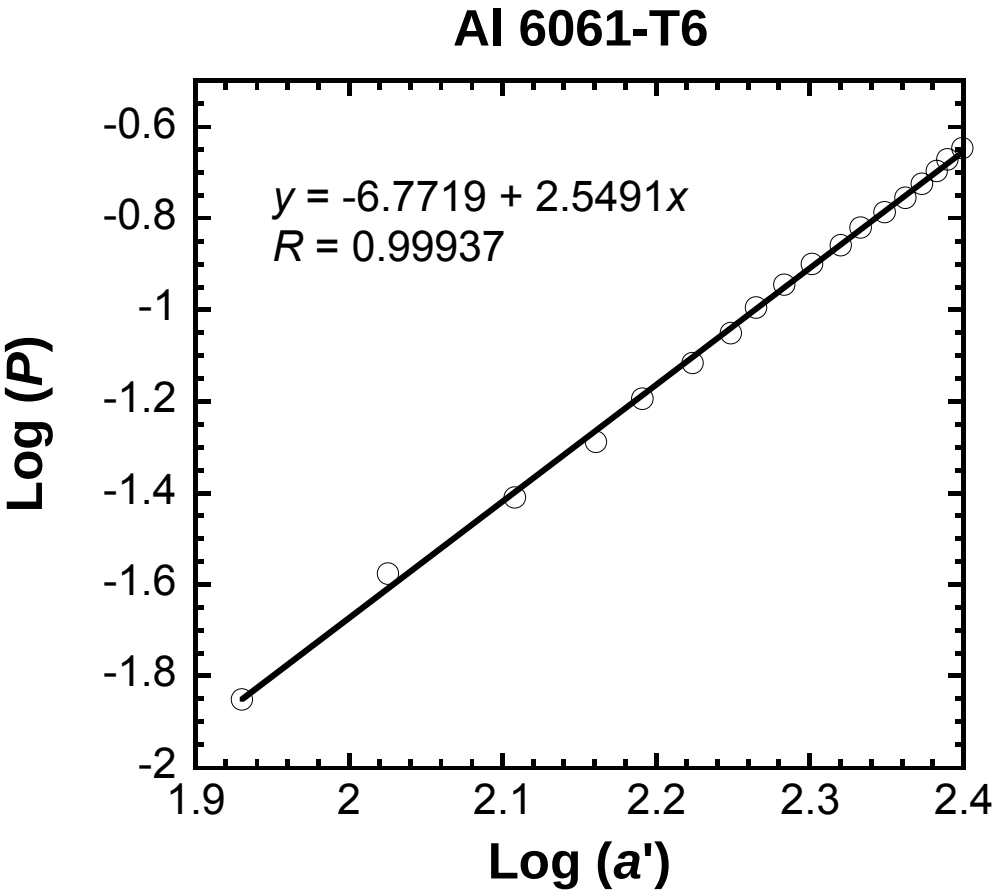

Figure 10. The linear regression of Log (*P*) vs. Log (*a*') used in the Field and Swain analysis. Based on the high fit correlation and a slope that lies between 2.0 and 2.6, the assumption of power law hardening would appear to be valid.

Here, we take this approach and calculate the contact area using Eq. (12) and stiffnesses determined from the stepwise loading procedure and an assumed modulus of 72.59 GPa.

Using the Tabor relations of $\sigma = p_m/2.8$ and $\varepsilon = 0.2a/R$ for the indentation data, Figure 11 compares the stress-strain behavior of 6061-T6 as determined by uniaxial tension and spherical indentation performed in accordance with the procedure outlined by Field and Swain. As illustrated by the plot, the indentation data are scattered, but predict a flow curve that is roughly 40% higher than the measured tensile data. Fitting the Field and Swain data beyond strains of 0.1 according the Hollomon power law expression yields $\sigma = 651.2\varepsilon^{0.135}$. In comparison to the actual tensile data, where the Hollomon relationship was found to be $\sigma = 432.0\varepsilon^{0.093}$, the indentation data overestimates both *K* and *n* by 51 and 45%, respectively. Fortuitously, using Eq. (40), the predicted yield strength is 312 MPa, an overestimation of only 14.3%.

Reducing the $\dot{P}/P$ data in the same fashion, where the stiffness was directly measured as opposed to being determined from the load-displacement data, produces results with significantly less scatter but ultimately the same problem. As shown in Figure 11, beyond the strain of 0.05, the $\dot{P}/P$ data overestimate the flow curve on the order of 30 to 40%. Strains below 0.05 correspond to displacements less than 17 nm, and thus represent data affected by the surface roughness as well as any contaminants or oxides on the surface. Fitting the $\dot{P}/P$ data beyond strains of 0.05 according to the Hollomon power law expression yields $\sigma = 707.2\varepsilon^{0.169}$. In comparison to the actual tensile data, the $\dot{P}/P$ indentation data overestimates both *K* and *n* by 64 and 82%, respectively. Using Eq. (40), the predicted yield strength is 275 MPa, an overestimation of only 0.73%, but the agreement is clearly fortuitous. The most meaningful comparison between the indentation and tensile data is reflected in the direct comparison of the stress-strain curves. Despite the excessive scatter in the Field and Swain data, both load-time histories predict flow stresses that are roughly 30 to 40% too

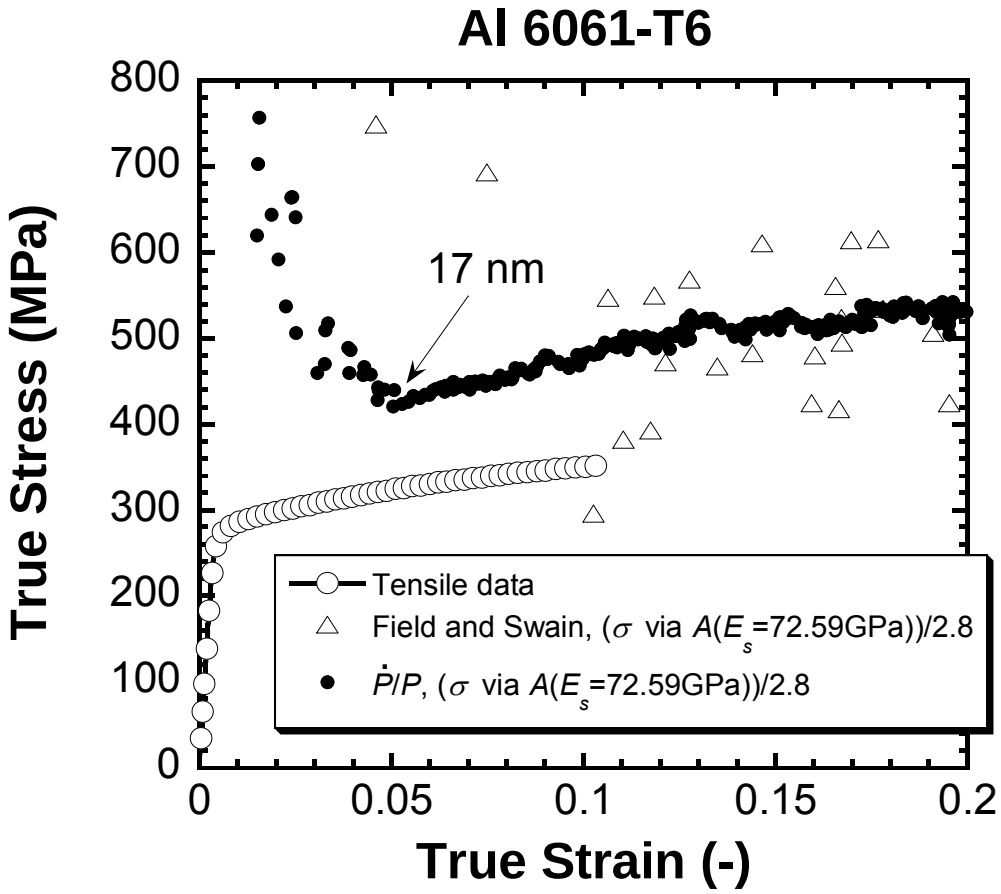

Figure 11. Comparison of the true stress vs. true strain behavior of Al 6061-T6 as determined by uniaxial tension and spherical indentation. The constraint factor is taken to be 2.8. The data below 17 nm is compromised by the effect of roughness and contaminants on the surface.

high. While a portion of this overestimation might be attributed to work hardening from the mechanical polishing, the work hardening ability of the alloy is not sufficient to fully account for the discrepancy between the indentation and tensile data.

One probable explanation for the difference is a mechanism completely ignored by each model in this investigation, specifically an indentation size effect due to the small radius of the spherical tip. In a series of carefully performed experiments in electropolished iridium, Swadener et al. [17] used five spheres ranging in radius from 14 to 1600 μm and clearly demonstrated an indentation size effect that scaled uniquely with the radius of the tip and not the depth of penetration, i.e. smaller radii produced greater hardnesses. Assuming some form of this mechanism is at work in the combination of 6061-T6 and a tip radius of 385 nm, Figure 12 shows the data can be rationalized by assuming a higher constraint factor of 3.7. This is consistent with the trends observed by Swadener et al. [17].

4.2 The method of W. Yu and J. P. Blanchard, 1996

In the limit of an elastic-plastic contact, Yu and Blanchard set out to develop analytical relationships among hardness, yield stress, elastic modulus, Poisson's ratio, and indenter geometry for materials idealized as elastic perfectly-plastic. By combining the pressure distribution predicted by elastic theory and the pressure distribution predicted by slip-line-field theory, Yu and Blanchard created an approximate pressure distribution that allowed them to determine the yield strength based on hardness measurements representative of an elastic-plastic contact. The result is a piecewise expression with natural limits that are consistent with an elastic contact as well as a rigid-plastic contact. Since the aluminum used in the experiments does not exhibit significant work hardening, Yu's model in the limit of the rigid plastic solution should apply. In addition, this solution has the added benefit of being a function of a/R, thus the constraint

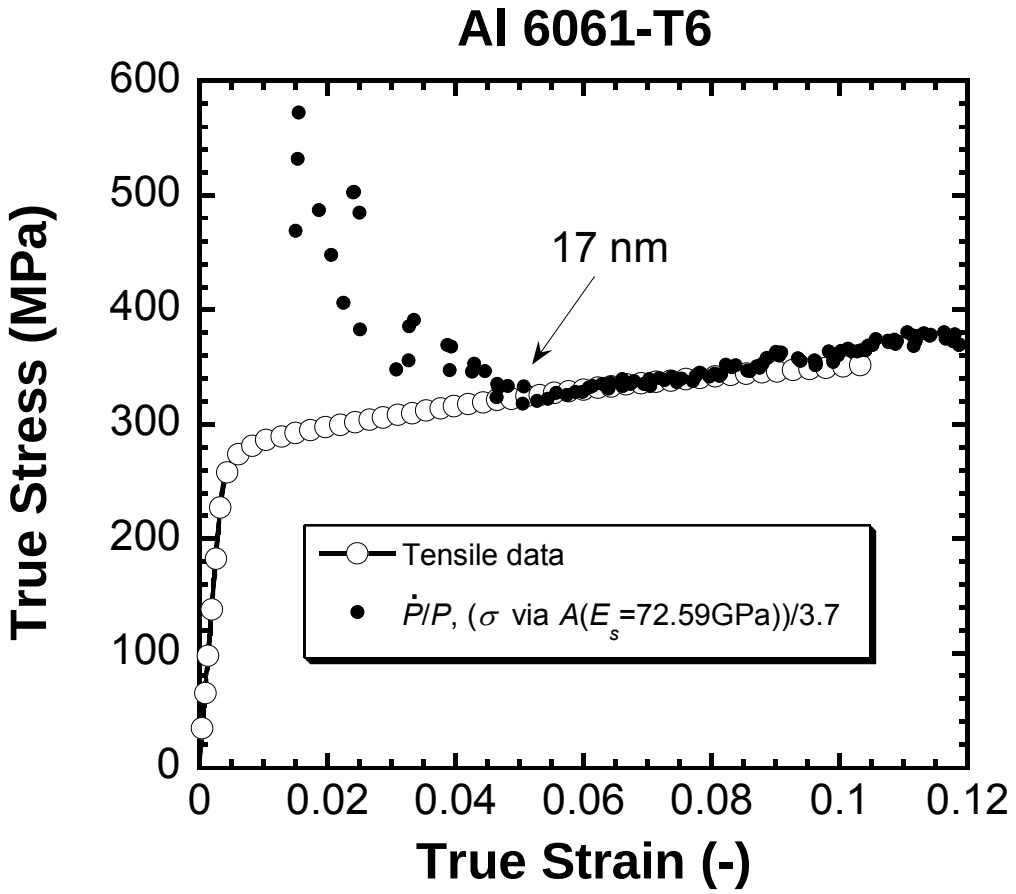

Figure 12. Comparison of the true stress vs. true strain behavior of Al 6061-T6 as determined by uniaxial tension and spherical indentation. The constraint factor is taken to be 3.7. The data below 17 nm is compromised by the affect of roughness and contaminants on the surface.

factor (p_m/σ_y , where p_m = P/A and A is the projected contact area) is not taken to be a constant. Integrating over their combined pressure distribution with respect to the radial position and making the appropriate substitutions, they find:

$$H = \frac{-18.94(R-0.1730a)\begin{pmatrix} R^2(\upsilon^2-1)^2\sigma_y{}^2 - 0.3459aR(\upsilon^2-1)^2\sigma_y{}^2 + \\ 0.0299a^2(\upsilon^4\sigma_y{}^2 - 2\upsilon^2\sigma_y{}^2 + \sigma_y{}^2 - 5.021E^2)\end{pmatrix}\sigma_y}{a^2E^2R} \quad (43)$$

where H is the hardness, and ν is Poisson's ratio. Clearly, implementing this equation requires determining the contact area, which Yu and Blanchard do not address in their proposed method. Of the several ways to determine the area, a simple and reliable expression that properly accounts for pile-up behavior is the stiffness equation, Eq. (12). Using Eq. (12) and stiffness data measured using the CSM technique, the hardness at approximately 20 nm of displacement was determined to be 1186.12 MPa. Based on this value and Eq. (43), the predicted yield strength is 424 MPa, an overestimation of approximately 55%.

There are numerous possible explanations for the discrepancy. The calculations were based on data at 20 nm of depth for the sole purpose of minimizing the impact of any work hardening. As shown in Figure 4, the Al does exhibit a small amount of work hardening, which is not accounted for in Yu's model. Therefore, the estimated yield stress is actually more representative of a flow stress. In addition, and as previously noted, it is certainly possible that the mechanical polishing may increase the near surface yield strength, thereby affecting the prediction of the yield strength in a manner that is unaccounted for in the modeling. However, in looking at the stress-strain behavior in Figure 4, it is clear that even if the mechanical polishing fully work hardened the near surface region, it would not be possible to increase the yield strength to 424 MPa. It is also important to note that at 20 nm of depth, surface roughness and oxidation may also affect the measurement.

4.3 The method of D. Ma, C. W. Ong, J. Lu, and J. He, 2003

Using dimensional and finite element analysis as their basis, Ma et al. developed a general methodology to determine the yield strength and hardening behavior of metals by instrumented indentation performed with a sphere. Two types of material behavior were considered: 1) elastic followed by Hollomon power law hardening, and 2) elastic with linear hardening. Given the previously noted power law hardening of 6061-T6, only the elastic with Hollomon power law hardening aspect of their proposed method will be discussed.

Their strategy for the evaluation of yield strength and hardening behavior is based on performing three experiments to maximum depths $h_m^{(i)}$, where i = 1 corresponds to a depth of 0.01R, i = 2 to 0.025R, and i = 3 to 0.05R. The loading portion of each of the three load-displacement curves is fitted according to the expression

$$P = P_m\left(\frac{h}{h_m}\right)^X \tag{44}$$

where P is the applied load, h is the measured depth, h_m is the maximum measured depth, P_m is a fit value representing the maximum load corresponding to h_m and X is the fitting exponent. The initial objective of their procedure is to determine the fit parameters P_m and X for each of the three loading curves.

Using the measured or known elastic modulus, the radius of the tip, and experimentally measured values for P_m and X, Figure 2 is used to determine an initial estimate of the yield strength and the work hardening behavior. Based on the experimentally acquired load-displacement data, the fit values obtained for P_m and X are presented in Figure 13. Of the three values obtained for X, 1.8417, 1.7786, and 1.2192, 1.8417 and 1.7786 do not fall within the range of values presented on the Y axis of Figure 2b. Using the elastic modulus obtained from the tensile experiments and the measured tip radius, the three values obtained for $P_m/(ER^2)$ are 0.037, 0.01, and 0.002; only 2 of the 3 values, 0.01 and 0.002, fall within the range of values presented on the Y axis of Figure 2a. Therefore, it

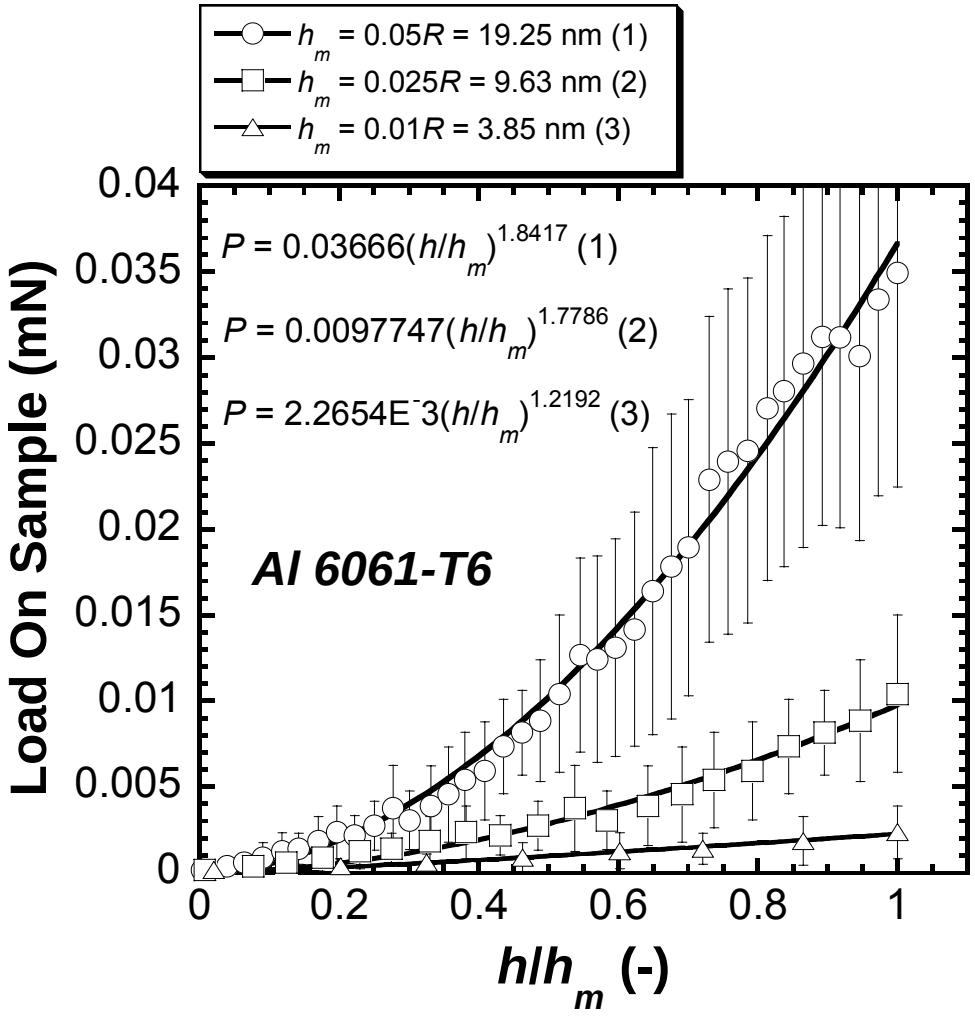

Figure 13. Averaged load vs. normalized displacement for Al 6061-T6. The error bars span one standard deviation about the mean. In accordance with Ma et al., the plotted curve fits provide the parameters P_m and X for each of the three experiments performed to nominal depths of 4, 10 and 20 nm.

is not possible to implement this procedure with the acquired load-displacement data.

Most likely, this procedure fails due to the affects of surface roughness. The depths to which these experiments were performed were approximately 4, 10 and 20 nm. AFM profiles, shown in Figure 9, indicate that the surface roughness is approximately 15 nm. By most standards for metallic samples, this is an excellent surface finish. Nevertheless, given that all of the models in this review make the assumption of intimate contact between the tip and sample, it should come as no surprise that the surface roughness makes it nearly impossible for any of the models to accurately reflect the physical geometry of the contact at depths that are on the order of the surface roughness. In addition, any contaminants or oxides on the surface as well as any unaccounted for effects of work hardening due to the mechanical polishing further serve to cloud the picture.

4.4 The method of Y. P. Cao, and J. Lu, 2004

Based on a priori knowledge of the elastic modulus and using a spherical indenter to perform experiments to depths of approximately 0.01R and 0.06R, the procedure proposed by Cao and Lu attempts to uniquely determine the yield strength and the work hardening index of the material by extending the representative strain as defined by Dao et al. [13] for sharp indentation to spherical indentation. The development of their model is based on the mechanical behavior of a bulk, homogeneous, isotropic material that behaves according to linear elasticity followed by Hollomon power law work hardening.

The constitutive relations used to describe the material behavior are $\sigma = E\varepsilon$ and $\sigma = K\varepsilon^n$. When $\sigma > \sigma_y$, the flow stress can also be expressed as

$$\sigma = \sigma_y \left(1 + \frac{E}{\sigma_y} \varepsilon_f \right)^n \tag{45}$$

where ε_f is the total effective strain accumulated beyond the yield strain.

Their measurement procedure consists of performing experiments to two different depths. Using their nomenclature, the recommended combination of depths is $h_{g,1} = 0.01R$ and $h_{g,2} = 0.06R$. The lower displacement limit is bound by the necessity to avoid deformation that is largely elastic. The upper limit is determined by the necessity to minimize the effects of friction, which become more prevalent as the depth of penetration increases.

The loads corresponding to $h_{g,1}$ and $h_{g,2}$ are recorded as $P_{g,1}$ and $P_{g,2}$. Based on their numerical analysis, the flow stresses corresponding to $P_{g,1}$ and $P_{g,2}$ are solved for according to the equation

$$P_g = \sigma_r h_g^2 \left[C_1 \ln^3\left(\frac{E_r}{\sigma_r}\right) + C_2 \ln^2\left(\frac{E_r}{\sigma_r}\right) + C_3 \ln\left(\frac{E_r}{\sigma_r}\right) + C_4 \right] \tag{46}$$

where σ_r is the flow stress and the coefficients C_1, C_2, C_3, and C_4 are a function of h_g/R and their respective values are provided in tabular from. The next step in their analysis is to calculate the effective strain from an expression again derived from their numerical analysis

$$\varepsilon_f = 0.00939 + 0.435\frac{h_g}{R} - 1.106\left(\frac{h_g}{R}\right)^2 . \tag{47}$$

By using Eqs. (46) and (47), the two experimental measurements effectively produce two points on the flow curve. Using Eq. 45 in the form of two equations and two unknowns, the yield strength can then be determined by solving the two equations simultaneously.

The experimental values obtained from our analysis were: $h_{g,1}$ = 4.2 nm, $P_{g,1}$ = 2.18 μN and $h_{g,2}$ = 23.3 nm, $P_{g,2}$ = 52.98 μN. Calculated from Eqs. (46) and (48), the resulting flow stresses and effective strains were: $\sigma_{r,1}$ = 4.24E+7 Pa, $\sigma_{r,2}$ = 2.98E+8 Pa, $\varepsilon_{f,1}$ = 0.0141, and $\varepsilon_{f,2}$ = 0.0316. For these values, there is no solution to Eq. (45) for $0 \le n \le 1$. In light of what is known about the surface

finish, again, it should come as no surprise that the method does not work since it is applied at depths that are less than the measured surface roughness.

5. Conclusions

The methods presented in this work all attempt to predict the yield strength of metals by instrumented indentation performed with a sphere. The mechanics principles from which these methods are based are the theory of elasticity, rigid-plastic deformation (slip-line-field theory), numerical analysis, and/or empirical observation. The sensitivity to experimental obstacles encountered in implementing these methods is a direct function of the depth at which experimental load-displacement data is acquired relative to the surface roughness, the depth of contaminants, the time necessary to perform the experiment, and the magnitude of the contact stiffness in comparison to the stiffness of the instrument load frame.

Despite Al 6061-T6 being well represented by the Hollomon power law relationship, the procedure outlined by Field and Swain overestimated the work hardening index n of the Al alloy. In accordance with their analysis, the overestimation of n necessarily underestimates the contact area, which precludes any meaningful estimate of the yield strength. In addition, using areas determined from the measured contact stiffness and an assumed elastic modulus, Field and Swain's procedure overestimated the tensile flow curve by roughly 40%. In comparison to the step-wise loading procedure suggested by Field and Swain, the data acquired by controlling $\dot{P}/P$ and measuring the elastic contact stiffness generated much more repeatable data, but the end result was effectively the same, a 30 to 40% overestimation of the tensile flow curve.

For Al 6061-T6 tested with a 385 nm radius sphere, the procedure proposed by Yu and Blanchard effectively reduces to the rigid plastic solution but with the added benefit of a constraint factor that is a function of a/R. Based on their proposed method, the predicted yield strength of Al 6061-T6 was overestimated by approximately 55%. While work hardening, whether from the mechanical polishing or the indentation itself, is in part responsible for this overestimation, it is not capable of fully accounting for this discrepancy. It is also

possible that an oxide layer on the surface contributes to the overestimation. However, if the $\dot{P}/P$ data in Figures 11 and 12 is any indication of when a single point contact is generated that is primarily controlled by the Al and not contaminants, then the data at 20 nm, which were used to make this prediction, should be consistent with the fundamental assumptions of the method.

The methods proposed to determine the yield strength of metals based on the numerical and finite element analyses of Ma et al. and Cao and Lu could not be implemented with the experimentally acquired data. Both models are based on the assumption of perfect contact between a perfectly spherical tip and a flat, homogeneous sample. Given the measured surface roughness of nominally 15 nm, it is simply not possible for these models to accurately reflect the physical geometry of the contact at depths less than ~15 nm, which is precisely where at least half of the indentation data were necessarily acquired due to the dimensions of the tip. In addition, any oxide layer on the surface also affects the experimental results in a manner that is not accounted for in the modeling. In summary, the experimental observations of this investigation suggest that roughness and contaminants on the surface are significant obstacles in applying the proposed methods of Ma et al. and Ca and Lu to experiments performed with a 385 nm radius sphere.

Collectively, these experimental observations suggest that it is experimentally quite difficult to make meaningful measurements of yield strength with a small sphere. Moreover, the work of Swadener et al. [17] suggests that estimating macroscopic flow and yield stresses from indentation data obtained with small spheres may be meaningless due to indentation size effects. Following Swadener's lead, the best way to test this hypothesis would be to perform experiments on an electropolished surface with several radii spheres. Any confirmation of this size effect should elicit serious concern because without accounting for it, it will not be possible to accurately predict the yield strength of metals based on indentation measurements performed with small radii spheres.

In accordance with Swadener's observations, small would be defined as a radius of approximately 122 μm or less.

References

References

[1] J. A. Brinell, J. Iron & Steel Inst. **59**, (1900), 243.

[2] D. Tabor, Hardness of Metals, Clarendon Press, Oxford, 1951.

[3] K. Johnson, J. Mech. Phys. Solids **18**, (1970), 115.

[4] J. S. Field and M. V. Swain, J. Mater. Res. **10**, 1 (1995), 101.

[5] W. Yu and J. P. Blanchard, J. Mater. Res. **11**, 9 (1996), 2358.

[6] D. Ma, C. W. Ong, J. Lu, and J. He, J. Appl. Phys. **94**, 1 (2003), 288.

[7] Y. P. Cao and J. Lu, Acta Mater. **52**, (2004), 4023.

[8] L. Kogut and K. Komvopoulos, J. Mater. Res. **19**, 12 (2004), 3641.

[9] H. Lee, J. H. Lee, and G. M. Pharr, J. Mech. Phys. Solids **53**, (2005), 2037.

[10] K. Johnson, Contact Mechanics, Cambridge University Press, 1989.

[11] J. S. Field and M. V. Swain, J. Mater. Res. **8**, 297 (1993).

[12] R. Hill, B. Storakers, and A. B. Zdunek, Proc. R. Soc. London **A423**, (1989), 301.

[13] M. Dao, N. Chollacoop, K. Van Vliet, T. Venkatesh, and S. Suresh, Acta Mater. **49**, (2001), 3899.

[14] S. Biwa and B. Storakers, J. Mech. Phys. Solids **43**, (1995), 1303.

[15] S. D. Mesarovic and N. A. Fleck, Proc. R. Soc. London **A455**, (1999), 2707.

[16] Y. J. Park and G. M. Pharr, Thin Solid Films **447**, 246 (2004).

[17] J. G. Swadener, E. P. George, and G. M. Pharr, J. Mech. Phys. Solids **50** (2002), 681.

Vita

Erik Gregory Herbert was born in Boston, MA on October 20 1969. He was raised in Massachusetts, New Hampshire, Pennsylvania, and Tennessee. He graduated from Anderson County High School in 1987. He received a B.A. in political science with a minor in business administration from the University of Tennessee, Knoxville, in 1992.

While working towards his masters, Erik has been a full time employee at the MTS Nano Instruments Innovation Center in Oak Ridge, TN. He is currently pursuing his doctorate in materials science and engineering at the University of Tennessee, Knoxville.